Theory of Random Copolymer Fractionation in Columns

CHAPTER *in* ADVANCES IN POLYMER SCIENCE · JULY 2010

Impact Factor: 1.99 · DOI: 10.1007/12_2010_92

1 AUTHOR:

Sabine Enders
Technische Universität Berlin

47 PUBLICATIONS **471** CITATIONS

SEE PROFILE

Adv Polym Sci (2011) 238: 271–328
DOI: 10.1007/12_2010_92

Published online: 31 July 2010

Theory of Random Copolymer Fractionation in Columns

Sabine Enders

Abstract Random copolymers show polydispersity both with respect to molecular weight and with respect to chemical composition, where the physical and chemical properties depend on both polydispersities. For special applications, the two-dimensional distribution function must adjusted to the application purpose. The adjustment can be achieved by polymer fractionation. From the thermodynamic point of view, the distribution function can be adjusted by the successive establishment of liquid–liquid equilibria (LLE) for suitable solutions of the polymer to be fractionated. The fractionation column is divided into theoretical stages. Assuming an LLE on each theoretical stage, the polymer fractionation can be modeled using phase equilibrium thermodynamics. As examples, simulations of stepwise fractionation in one direction, cross-fractionation in two directions, and two different column fractionations (Baker–Williams fractionation and continuous polymer fractionation) have been investigated. The simulation delivers the distribution according the molecular weight and chemical composition in every obtained fraction, depending on the operative properties, and is able to optimize the fractionation effectively.

Keywords Continuous thermodynamics · Fractionation in column · Theory of copolymer fractionation

S. Enders
TU Berlin, Fachgebiet "Thermodynamik und Thermische Verfahrenstechnik", TK 7, Strasse des 17. Juni 135, 10623 Berlin, Germany
e-mail: Sabine.Enders@TU-Berlin.de

Contents

Symbols

f	Segment-molar activity coefficient
F	Fraction
k	Reciprocal to the uniformity, see (15)
m	Number of stages in the fractionation-column
P	Pressure
r	Segment number
R	Ideal gas constant
T	Temperature
U	Nonuniformity (30)
v	Number of volume increments in the Baker–Williams column
W	Intensive two-dimensional distribution function
w	Extensive two-dimensional distribution function
X	Segment fraction
y	Chemical composition of statistical copolymers
Z	Segment fraction of the solvent in the solvent + nonsolvent mixture

Abbreviations

CF	Cross-fractionation
CPF	Continuous polymer fractionation
CSF	Continuous spin fractionation
EA	Extraction agent
EVA	Ethylene vinyl acetate copolymer
FD	Feed in continuous polymer fractionation
GPC	Gel permeation chromatograph

SEC Size exclusion chromatography
SPF Successive precipitation fractionation
SSF Successive solution fractionation

Greek Symbols

μ Segment-molar chemical potential
Γ Gamma function
γ Parameter defined in (5)
χ Flory–Huggins interaction parameter
ε Parameter of the Stockmayer distribution function (15) describing the broadness of the chemical heterogeneity
ϕ Quotient of the total amount of segments in phase II and in phase I
ρ Abbreviation, defined in (9) and (11)
η Parameter of the Baker–Williams column in (45)
τ Parameter of the Baker–Williams column in (45)
θ Parameter of the Baker–Williams column in (45)
λ Parameter of the Baker–Williams column in (45)

Subscripts

A Solvent
E Excess quantity
M Mixture
m Number of stages in the fractionation-column
Max Number of maximal stage in CPF-column
i Component i in the mixture
N Number-average quantity
n Number of volume increment in the Baker–Williams column
W Mass-average quantity

Superscripts

I Phase I
II Phase II
F Feed phase

1 Introduction

Synthetic copolymers are always polydisperse, i.e., they consist of a large number of chemically similar species with different molar masses and different chemical compositions. Owing to this polydispersity, characterization of copolymers does usually not provide the number of individual molecules or their mole fraction, mass fraction, etc. but requires the use of continuous distribution functions or their averages. Continuous thermodynamics, developed by Rätzsch and Kehlen [1], can be directly applied to the calculation of thermodynamic properties, including phase equilibria, because this theoretical framework is based completely on continuous distribution functions, which include all the information about these functions and allow an exact mathematical treatment of all related thermodynamic properties. Continuous thermodynamics have been used for calculation of phase equilibria of systems containing two-dimensional distributed copolymers [1–8]. The purpose of this contribution is the application of continuous thermodynamics to copolymer fractionation according to the chemical composition and molecular weight.

Basic research concerning the physical–chemical behavior of polymer solutions is overwhelmingly confined to a few polymers, like polystyrene, that can be polymerized anionically to yield products of narrow molecular weight distribution. One of the reasons for this choice lies in the fact that most polymer properties are not only dependent on the degree of polymerization but are also strongly affected by the broadness of the molecular weight distribution. It is desirable to produce nearly monodisperse polymers. One possibility for doing so is the use of polymer fractionation. Fractionations of polymers are carried out for two different purposes. One purpose is the analytical determination of the molar weight distribution and the other is the preparation of fractions large enough in size to permit study of their properties. In analytical fractionation, the amount of initial polymer is usually small. The fractions do not need to be separated and are often characterized online in automated fractional dissolution procedures. Some column techniques are in use that are based on thermodynamic equilibrium principles and make use of either liquid/liquid or liquid/solid phase separations. In preparative polymer fractionation, scaling-up problems are the main issue, because the necessary amount of initial polymer increases considerably when the purity requirements of the fractions are raised [9–11].

The fractionation of copolymers presents a special problem. For a chemically homogeneous polymer, solubility only depends on molecular weight distribution. In the case of chemically inhomogeneous materials, such as copolymers, solubility is determined by the molecular weight distribution, as well as by chemical composition. In the case of copolymers, both distributions can change during the course of fractionation. The efficiency of any given copolymer fractionation can be estimated from the data on the heterogeneity of fractions in molecular weight (molecular heterogeneity) and in composition (composition heterogeneity).

One of the long-sought “Holy Grails” of polymer characterization has been the simultaneous determination of polymer composition as a function of molecular

weight distribution. The combination of a solvent evaporative interface between a gel permeation chromatograph (GPC) and a Fourier transform infrared spectrometer has provided one useful solution to the problem of determining polymer composition as a function of molecular weight for different polymers [12]. Poly (ethylene-*co*-acrylic acid) copolymers were fractionated with supercritical propane, butane, and dimethyl ether [13]. It was possible to carry out the fractionation with respect to the molecular weight using increasing pressure at constant temperature. Additionally, it was possible to fractionate these acid copolymers with respect to chemical composition by first using one of the poor quality solvents (propane or butane) that solubilized the nonpolar ethylene-rich oligomers, and then using dimethyl ether, a very strong solvent for these acid copolymers, to solubilized the acid-rich oligomers. Other examples for the application of supercritical fluids can be found in the literature [14, 15].

One of the most common methods for carrying out analytical polymer fractionation is that of size-exclusion chromatography (SEC), also known as GPC. The polymer solution is passed through a column packed with porous gel beads. The pores have radii comparable in magnitude to the root-mean-square radius of gyration of an average polymer molecule in the sample. The larger molecules are preferentially excluded from the pores, inside which their more extended conformations are forbidden, and are eluted from the column earlier than the smaller molecules. Online detection of the eluent invariably involves refractivity to monitor polymer concentration, and might include light scattering and viscosity. This method was applied to characterize different polymers, like styrene–acrylonitrile copolymers [16–18], α-methylstyrene–acrylonitrile copolymers [19], styrene–methyl methacrylate copolymers [18, 20, 21], styrene–ethyl methacrylate copolymer [22–24], styrene–2 methoyethyl methacrylate copolymer [25], and ethylene terephthalate–tetramethylene ether [26]. Other methods developed for the characterization of copolymers are: fractionation in demixing solvents [27–29], combination of GPC with temperature-programmed column fractionation (TPCF) [30, 31], interaction chromatography [32], column elution method [33], temperature rising elution fractionation (TREF) [34, 35], combination of SEC with precipitation chromatography [36, 37], and crystallization [38, 39].

Within this contribution, we focus our attention on two methods, namely the Baker–Williams fractionation (BW) [40, 41] and continuous polymer fractionation (CPF) [42]. The BW method leads to fractions with a very low nonuniformity and is deemed to be the most effective technique [43, 44]. CPF allows the isolation of fractions on the 100 g scale.

Only a few papers can be found in the literature that deal with theoretical questions on this topic. With the help of continuous thermodynamics, a theory to model stepwise fractionation of homopolymers was developed [45–47]. This theoretical framework could be extended to fractionation in columns [48–50]. The application of the developed theory was able to contribute to the improvement of the fraction technique [49]. Folie [51] studied the fractionation of copolymers. In his theoretical framework, the polymer was described by pseudocomponents with respect to the molecular weight; however, the polydispersity with respect to the

chemical composition was neglected. First, Litmanovich and Shtern [52] modeled stepwise copolymer fractionation, where both polydispersities were considered. Later, Ogawa and Inaba [53] also suggested a similar model.

This contribution aims at the development of a theoretical tool for optimization of copolymer fractionation in columns, where both polydispersities are completely taken into account.

2 Theory

2.1 Liquid–Liquid Phase Equilibrium of Copolymer Solutions

Fractionations are usually carried out using a solvent (A), a nonsolvent (B) and the polymer to be fractionated. This means that, for phase equilibrium calculations, a ternary system must be investigated. Due to the very large number of different chemical species, the composition of polydisperse systems is not described by the mole fraction of the individual components, but by a continuous distribution function. In the case of statistical copolymers, a two-dimensional distribution function according the molecular mass and the chemical composition must be used. Usually in polymer thermodynamics, all molecules are imagined to be divided into segments of equal size. With a standard segment defined as the ratio of the van der Waals volume of the considered species and the van der Waals volume of an arbitrary chosen species (for instance one of the solvents or one of the monomers), a segment number r can be defined for each kind of molecule. The introduction of the segment number leads to segment-molar physical quantities. The chemical composition of a copolymer, built up from two different monomers, can be described by the variable y. It is given by the ratio of the segment number of one monomer and the sum of the segment numbers of both monomers, and hence y is related to the amount of one monomer in the copolymer. The intensive distribution function, $W(r, y)$, has to fulfill the normalization condition:

$$\int_0^\infty \int_0^1 W(r,y)\mathrm{d}y\mathrm{d}r = 1. \tag{1}$$

$W(r, y)\mathrm{d}y\mathrm{d}r$ represents the segment fraction of all copolymer species having segment numbers between r and $r + \mathrm{d}r$ and chemical compositions between y and $y + \mathrm{d}y$.

Due to the polydispersity, the demixing behavior becomes much more complicated for a polydisperse polymer in comparison with a monodisperse polymer, as shown in Fig. 1. The binodal curve in this system splits into three kinds of curves: a cloud-point curve, a shadow curve, and an infinite number of coexistence curves. The meaning of these curves becomes clear if one considers the cooling process.

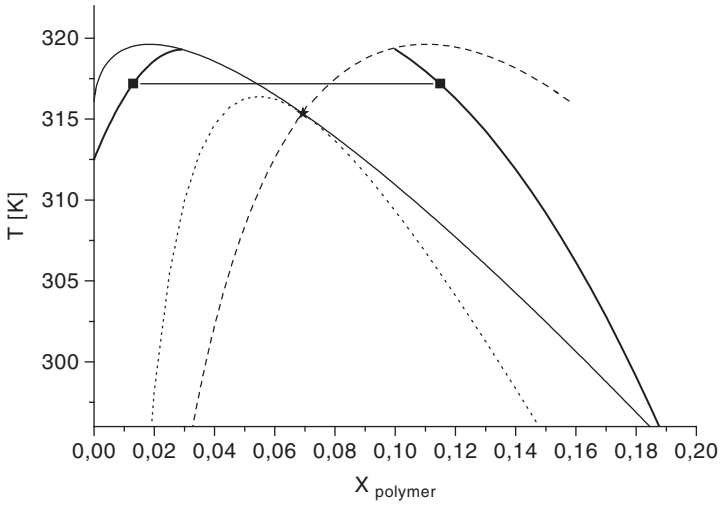

Fig. 1 Schematic liquid–liquid phase diagram for a polydisperse polymer in a solvent: *Solid line* cloud-point curve, *broken line* shadow curve, *dotted line*: spinodal curve, *star* critical point, *thick lines* coexisting curves, *solid line with squares* tie line, $X_{polymer}$ segment fraction of polymer

When reaching the cloud-point curve, at lowering of the temperature, the overall polymer content of the first droplets of the precipitated phase does not correspond to a point on the cloud-point curve but to the corresponding point on the shadow curve. With further lowering of the temperature, the two coexisting phases do not change their overall polymer content according to the cloud-point curve or to the shadow curve but according to the related branches of the coexistence curves. The overall polymer content of the coexisting phases is given by the intersection points of the horizontal line, at the considered temperature, with these branches (tie line in Fig. 1). The coexistence curves are usually not closed curves but are divided into two branches beginning at corresponding points of the cloud-point curve and the shadow curve. Only if the composition of the initial homogeneous phase equals that of the critical point is a closed coexistence curve obtained, whose extremum is the critical point. Moreover, at this point, the cloud-point curve and shadow curve intersect. It can be seen from Fig. 1 that, for solutions of polydisperse polymers, the critical point is not located at the extremum of the cloud-point curve or of the shadow curve. This is in contrast to strictly binary systems where the cloud-point curve, shadow curve, and all coexistence curves become identical.

Homopolymers in coexisting phases show different molar weight distributions, which are also different from that of the initial homogeneous system (Fig. 2). This effect is called the fractionation effect and can be used for the production of tailor-made polymers. The phase with a lower polymer concentration (sol phase) contains virtually only the polymers with a lower molecular weight. Consequently, polymers having a high molecular weight remain in the concentrated phase (gel phase). The cloud-point curve always corresponds to the molecular weight distribution of the

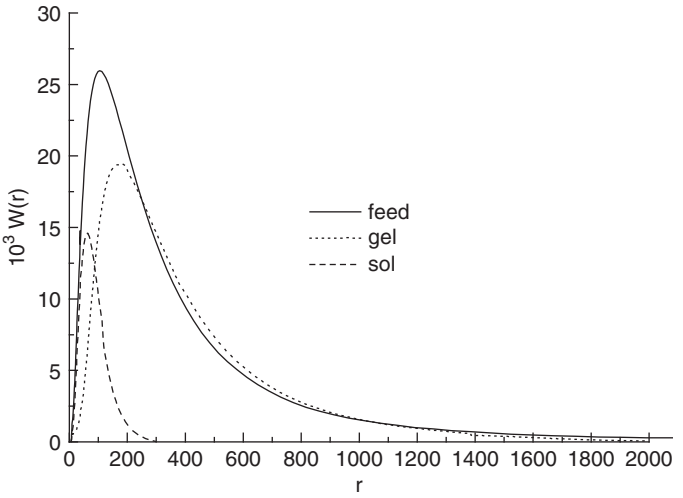

Fig. 2 Fractionation effect for homopolymers

initial polymer, but the first droplets of the formed coexisting new phase never do (with the exception of the critical point) and, hence, they are not located at the cloud-point curve but on the shadow curve. In the case of statistical copolymers, the distribution function according to the chemical composition also differs in the two phases; however, how this distribution changes cannot be predicted a priori. The residence (sol or gel phase) of the molecules with a high value of y depends on the thermodynamic properties of the selected solvent mixture.

To perform phase equilibrium calculations, the starting point is the segment-molar chemical potential, m_i, related to the segment-molar Gibbs free energy of mixing. According to the well-known Flory–Huggins lattice theory [54], the segment-molar chemical potential (μ_i) for the solvents A and B reads:

$$\mu_i = \mu_{i0}(T,P) + RT\left[\frac{1}{r_i}\ln X_i + \frac{1}{r_i} - \frac{1}{r_\mathrm{M}}\right] + RT\ln f_i \quad i = \mathrm{A},\mathrm{B}, \tag{2}$$

where the first term represents the segment-molar chemical potential of the pure solvents at system temperature T and system pressure P. The second term on the right hand side is the Flory–Huggins contribution (with $f_i = 1$), accounting for the difference in molecular size. In order to describe the deviation from a Flory–Huggins mixture (with $f_i = 1$), the segment-molar activity coefficients, f_i, are introduced. The number-average segment number, r_M, in (2) is for a ternary system, built up from solvent, nonsolvent, and copolymer, and is given by:

$$\frac{1}{r_\mathrm{M}} = \frac{X_\mathrm{A}}{r_\mathrm{A}} + \frac{X_\mathrm{B}}{r_\mathrm{B}} + \frac{X}{r_\mathrm{N}} = \frac{X_\mathrm{A}}{r_\mathrm{A}} + \frac{X_\mathrm{B}}{r_\mathrm{B}} + \int_0^\infty \int_0^1 \frac{XW(r,y)}{r}\,\mathrm{d}y\mathrm{d}r, \tag{3}$$

where r_N is the number-average segment number of the copolymer. The segment-molar chemical potential for the copolymer species thus depends on the segment number, r, and the chemical composition, y [4, 6]:

$$\mu(r,y) = \mu_0(T,P,r,y) + RT\left[\frac{1}{r}\ln XW(r,y) + \frac{1}{r} - \frac{1}{r_M}\right] + RT\ln f(r,y). \quad (4)$$

Similar to (2), in (4) the first term is the segment-molar chemical potential of the pure copolymer species with the segment number r and the chemical composition y. The second term displays the Flory–Huggins term and the last term characterizes the deviation from the Flory–Huggins mixture, where the segment-molar activity coefficient can, in principle, depend on the molecular weight and the chemical composition. Whereas the dependence on molecular weight can often be neglected, the dependence on chemical composition plays an important role [3, 6].

Rätzsch et al. [3] suggested the following model for the segment-molar excess Gibbs free energy of mixing (G^E) in order to describe the deviation from the Flory–Huggins mixture:

$$\frac{G^E}{RT} = X_A X\frac{\chi_{AP}}{T}(1+p_A X)(1+\gamma_A y_W) + X_B X\frac{\chi_{BP}}{T}(1+p_B X)(1+\gamma_B y_W) + X_A X_B\frac{\chi_{AB}}{T}, \quad (5)$$

where y_W is the weight-average chemical composition. This quantity can be calculated using:

$$y_W = \int_0^\infty\int_0^1 yW(r,y)\mathrm{d}y\mathrm{d}r. \quad (6)$$

The influence of the chemical composition in (5) can be derived using a simplified version of Barker's lattice theory [55]. The most important consequence of (5) is the fact that the segment-molar excess Gibbs free energy of mixing and, hence, the activity coefficients depend only on the average value (y_W) of the distribution function, but not on the distribution function itself. In continuous thermodynamics, the phase equilibrium conditions read:

$$\mu_i^I = \mu_i^{II} \quad \mu^I(r,y) = \mu^{II}(r,y) \quad i = A,B. \quad (7)$$

Here, the phase equilibrium condition for the copolymer holds for all polymer species within the total segment number and chemical composition range of the system. This equation is valid for the total interval of the values of the identification variables r and y found in the system. Replacing the segment-molar chemical potentials for the solvents in (7) according to (2) and rearranging results in:

$$X_i^{II} = X_i^I\exp(r_i\rho_i) \quad i = A,B, \quad (8)$$

where the abbreviation ρ_i can be calculated using:

$$\rho_i = \frac{1}{r_{\mathrm{M}}^{\mathrm{II}}} - \frac{1}{r_{\mathrm{M}}^{\mathrm{I}}} - \ln f_i^{\mathrm{II}} + \ln f_i^{\mathrm{I}} \quad i = \mathrm{A}, \mathrm{B}. \tag{9}$$

The activity coefficients in (9) can be derived using standard thermodynamics in combination with (5). The replacement of the segment-molar chemical potential of the copolymer species in (7) according (4) leads to:

$$X^{\mathrm{II}} W^{\mathrm{II}}(r, y) = X^{\mathrm{I}} W^{\mathrm{I}}(r, y) \exp(r\rho(y)), \tag{10}$$

where the abbreviation ρ is given by:

$$\rho(r, y) = \frac{1}{r_{\mathrm{M}}^{\mathrm{II}}} - \frac{1}{r_{\mathrm{M}}^{\mathrm{I}}} - \ln f^{\mathrm{II}}(y) + \ln f^{\mathrm{I}}(y). \tag{11}$$

Equation (10) is valid for all r and y values found in the system and permits the calculation of an unknown distribution function, $W^{\mathrm{II}}(r, y)$. The activity coefficients in (11) can be derived using standard thermodynamics in combination with (5). Integration of (10) and applying the normalization condition (1) results in:

$$X^{\mathrm{II}} = \int_0^\infty \int_0^1 X^{\mathrm{I}} W^{\mathrm{I}}(r, y) \exp(r\rho(r, y)) \mathrm{d}y \mathrm{d}r. \tag{12}$$

To deal with the problem of calculation of the cloud-point curve and the corresponding shadow curve, the temperature of a given phase I is changed at constant pressure until the second phase II is formed. Thus, the unknowns of the problem are the equilibrium temperature, T, the composition of the second phase, X^{II} and $X_{\mathrm{A}}^{\mathrm{II}}$, and the distribution function, $W^{\mathrm{II}}(r, y)$. To calculate them, the phase equilibrium conditions (8) and (12) are used. In this system of equations, the unknown distribution function $W^{\mathrm{II}}(r, y)$ and the other scalar unknowns T, X^{II}, and $X_{\mathrm{A}}^{\mathrm{II}}$ are connected; however, the unknown distribution function $W^{\mathrm{II}}(r, y)$ occurs only with the average values $r_{\mathrm{N}}^{\mathrm{II}}$ and $y_{\mathrm{W}}^{\mathrm{II}}$. This situation allows a separation of the problem of the unknown distribution function by considering $r_{\mathrm{N}}^{\mathrm{II}}$ and $y_{\mathrm{W}}^{\mathrm{II}}$ as additional scalar unknowns and their defining equations:

$$\frac{X^{\mathrm{II}}}{r_{\mathrm{N}}^{\mathrm{II}}} = \int_0^\infty \int_0^1 \frac{X^{\mathrm{I}} W^{\mathrm{I}}(r, y)}{r} \exp(r\rho(r, y)) \mathrm{d}y \mathrm{d}r \tag{13}$$

and

$$y_{\mathrm{W}}^{\mathrm{II}} X^{\mathrm{II}} = \int_0^\infty \int_0^1 y X^{\mathrm{I}} W^{\mathrm{I}}(r, y) \exp(r\rho(r, y)) \mathrm{d}y \, \mathrm{d}r, \tag{14}$$

as additional scalar equations. For calculation of the cloud-point curve and the shadow curve, five equations, namely (8) and (12)–(14), must be solved simultaneously. Furthermore, for numerical calculations, r_N^{II} might be eliminated by means of (8) and (9). The unknown distribution function of the copolymer, $W^{II}(r, y)$, in the shadow phase can be calculated using (10).

Rätzsch et al. [3, 6] could demonstrate that the integrals occurring in (12)–(14) can be solved analytically under certain circumstances, namely if the Stockmayer distribution function [56] is used:

$$W(r,y) = \frac{k^{k+1}}{r_N \Gamma(k+1)} \left(\frac{r}{r_N}\right)^k \exp\left(-k\frac{r}{r_N}\right) \sqrt{\frac{r}{2\pi\varepsilon}} \exp\left(-\frac{r(y-y_W)^2}{2\varepsilon}\right). \qquad (15)$$

The first two factors in (15) are a generalized Schulz–Flory distribution with respect to the segment number r. The parameters are k, describing the nonuniformity, and r_N the number-average segment number. Γ is the Γ function. The last two factors are a Gaussian distribution with respect to the chemical composition y, with a standard deviation of $\sqrt{\varepsilon/r}$. The parameters of the Gaussian distribution are the weight-average chemical composition, y_W, and the quantity ε describing the broadness of the chemical heterogeneity. They can be estimated by the kinetic copolymerization parameters because (15) was derived by the kinetics of statistical copolymerization [56]. However, in reality, many copolymers show broad and asymmetric chemical distributions that are not of the Stockmayer type (15). Rätzsch et al. [6] suggested the replacement of the Gaussian distribution function in (15) by the Γ function. The combination of the Γ function for the chemical heterogeneity with the Schulz–Flory distribution for the heterogeneity of the molecular weight reads:

$$W(r,y) = \frac{k^{k+1}}{r_N \Gamma(k+1)} \left(\frac{r}{r_N}\right)^k \exp\left(-k\frac{r}{r_N}\right) \frac{\Gamma(\alpha+\beta+2)}{\Gamma(\alpha+1)\Gamma(\beta+1)} y^\alpha (1-y)^\beta, \qquad (16)$$

where α and β are the parameters describing the distribution of the chemical composition. For the special case $\alpha = \beta$, a symmetrical distribution function results. The value of α indicates the broadness of the distribution, where the limiting case $\alpha \to \infty$ leads to a monodisperse copolymer with respect to the chemical composition. This distribution function displays a large flexibility and allows for the description of asymmetrical distributions. The most important difference between both distribution functions is that in (15) the chemical heterogeneity depends on the segment number, whereas in (16) the chemical composition does not depend on the segment number.

An alternative approach to the calculation of the cloud-point and shadow curve is the application of an equation of state (i.e., [7, 57–60]). The stability conditions in terms of spinodal and critical point are given by Browarzik and Kehlen [61].

To calculate the coexistence curve where a feed phase F splits into the coexisting phases I and II, the mass balance of the copolymer:

$$X^{\mathrm{F}}W^{\mathrm{F}}(r,y) = (1-\phi)X^{\mathrm{I}}W^{\mathrm{I}}(r,y) + \phi X^{\mathrm{II}}W^{\mathrm{II}}(r,y) \tag{17}$$

must also be applied [3, 6]. The quantity ϕ is the quotient of the total amount of segments in phase II and in feed phase F and equals the fraction of the feed volume that forms phase II. The mass balance for the solvents reads:

$$X_i^{\mathrm{F}} = (1-\phi)X_i^{\mathrm{I}} + \phi X_i^{\mathrm{II}} \quad i = \mathrm{A}, \mathrm{B}. \tag{18}$$

Additionally, two balance equations related to the moments of the distribution function can be formulated:

$$\frac{X^{\mathrm{F}}}{r_{\mathrm{N}}^{\mathrm{F}}} = (1-\phi)\frac{X^{\mathrm{I}}}{r_{\mathrm{N}}^{\mathrm{I}}} + \phi\frac{X^{\mathrm{II}}}{r_{\mathrm{N}}^{\mathrm{II}}} \tag{19}$$

and

$$y_{\mathrm{W}}^{\mathrm{F}}X^{\mathrm{F}} = (1-\phi)y_{\mathrm{W}}^{\mathrm{I}}X^{\mathrm{I}} + \phi y_{\mathrm{W}}^{\mathrm{II}}X^{\mathrm{II}}. \tag{20}$$

Besides the feed, two of the three variables T, P, and ϕ have to be specified. Starting with the phase equilibrium conditions (8) and (9), the balances (17)–(20) can be used to eliminate the quantities referring to one of the two coexisting phases (for instance phase I), which leads to:

$$X_i^{\mathrm{II}} = \frac{X_i^{\mathrm{F}}}{\phi + (1-\phi)\exp(-r_i\rho_i)} \quad i = \mathrm{A}, \mathrm{B}. \tag{21}$$

$$X^{\mathrm{II}}W^{\mathrm{II}}(r,y) = \frac{X^{\mathrm{F}}W^{\mathrm{F}}(r,y)}{\phi + (1-\phi)\exp(-r\rho_{\mathrm{B}}(r,y))} = \frac{K(r,y)X^{\mathrm{F}}W^{\mathrm{F}}(r,y)}{\phi}, \tag{22}$$

where the precipitation rate $K(r,y)$ is defined as [46]:

$$K(r,y) = \frac{\phi X^{\mathrm{II}}W^{\mathrm{II}}(r,y)}{X^{\mathrm{F}}W^{\mathrm{F}}(r,y)} = \frac{\phi}{\phi + (1-\phi)\exp(-r\rho(r,y))}. \tag{23}$$

Integration of (22) results in:

$$X^{\mathrm{II}} = \int_r \int_y \frac{K(r,y)X^{\mathrm{F}}W^{\mathrm{F}}(r,y)}{\phi}\mathrm{d}y\mathrm{d}r. \tag{24}$$

The number-average segment number in the second phase is given by:

$$\frac{X^{\mathrm{II}}}{r_{\mathrm{N}}^{\mathrm{II}}} = \int_r \int_y \frac{K(r,y)X^{\mathrm{F}}W^{\mathrm{F}}(r,y)}{r\phi}\mathrm{d}y\mathrm{d}r. \tag{25}$$

The weight-average chemical composition in the second phase is given by:

$$y^{\mathrm{II}}X^{\mathrm{II}} = \int_r \int_y \frac{yK(r,y)X^{\mathrm{F}}W^{\mathrm{F}}(r,y)}{\phi}\mathrm{d}y\mathrm{d}r. \tag{26}$$

In contrast to the cloud-point problem, the integrals occurring in (24)–(26) cannot be solved analytically. In order to calculate the coexisting curves, (21) and (24)–(26) must be solved simultaneously, where the occurring integrals must be estimated using a numerical procedure. If the quantities of feed solution (X^{F}, $W^{\mathrm{F}}(r, y)$, and $X_{\mathrm{A}}^{\mathrm{F}}$) are known, the unknowns are the temperature T (or the quantity ϕ); the polymer concentration in the second phase, X^{II}; the solvent concentration in the second phase, $X_{\mathrm{A}}^{\mathrm{II}}$; the number-average segment number in the second phase, $r_{\mathrm{N}}^{\mathrm{II}}$; and the weight-average chemical composition, $y_{\mathrm{W}}^{\mathrm{II}}$. The corresponding quantities of the first phase can be estimated using the balance equations (17)–(20). If the selected G^{E} model is not dependent on the segment number, a simplification is possible. Inserting the solvent equilibrium conditions [(21) with $i = \mathrm{B}$] the system can be reduced to four equations by eliminating, $r_{\mathrm{N}}^{\mathrm{II}}$. The final equation reads:

$$\begin{aligned} 0 = &\int_r \int_y \frac{K(r,y)X^{\mathrm{F}}W^{\mathrm{F}}(r,y)}{r\phi}\mathrm{d}y\mathrm{d}r - \frac{1}{r_{\mathrm{M}}^{\mathrm{F}}} + \frac{X_{\mathrm{A}}^{\mathrm{II}}}{r_{\mathrm{A}}} + \frac{X_{\mathrm{B}}^{\mathrm{II}}}{r_{\mathrm{B}}} - (1-\phi) \\ &\times \left[\frac{1}{r_{\mathrm{B}}}\ln\left(\frac{X_{\mathrm{B}}^{\mathrm{II}}}{X_{\mathrm{B}}^{\mathrm{I}}}\right) + \ln f_{\mathrm{B}}^{\mathrm{II}} - \ln f_{\mathrm{B}}^{\mathrm{I}}\right], \end{aligned} \tag{27}$$

where $p(r, y)$ in (23) is replaced by $p(y)$ and can be calculated by:

$$\rho(y) = \frac{1}{r_{\mathrm{B}}}\ln\left(\frac{X_{\mathrm{B}}^{\mathrm{II}}}{X_{\mathrm{B}}^{\mathrm{I}}}\right) + \ln f_{\mathrm{B}}^{\mathrm{II}} - \ln f_{\mathrm{B}}^{\mathrm{I}} - \ln f^{\mathrm{II}}(y) + \ln f^{\mathrm{I}}(y) \tag{28}$$

and

$$\rho_{\mathrm{A}} = \frac{1}{r_{\mathrm{B}}}\ln\left(\frac{X_{\mathrm{B}}^{\mathrm{II}}}{X_{\mathrm{B}}^{\mathrm{I}}}\right) + \ln f_{\mathrm{B}}^{\mathrm{II}} - \ln f_{\mathrm{B}}^{\mathrm{I}} + \ln f_{\mathrm{A}}^{\mathrm{I}} + \ln f_{\mathrm{A}}^{\mathrm{II}}. \tag{29}$$

The coexisting-curve problem is now given by (21) with $i = \mathrm{A}$, (24), (26), and (27), where (28) and (29) can be used to compute $\rho(y)$ and ρ_{A}.

Fractionation efficiency is the central feature in the calculation of fractionation, and must be judged by an objective criterion. For fractionation with respect to the molar mass, the uniformity of every fraction, i, can be used. The uniformity (U_i) is defined by:

$$U_i = \frac{M_{\mathrm{W},i}}{M_{\mathrm{N},i}} - 1 = \frac{r_{\mathrm{W},i}}{r_{\mathrm{N},i}} - 1. \tag{30}$$

The more U deviates from zero, the less efficient is the fractionation. The fractionation with respect to the chemical composition is characterized by the distribution function itself.

Thermodynamic principles are relevant to separation processes that make use of the distribution of macromolecules between two phases. These two phases may form a partially miscible system. The diluted phase is called sol phase I, and the polymer-rich phase is the gel phase II. The distribution coefficient depends on molar mass and on chemical composition. Figure 2 depicts the distribution functions in the sol and gel phases. Fractionation can be achieved in a single solvent by a change of temperature, but it is often more practical to vary the solvent quality by using a binary solvent mixture composed of a nonsolvent and a good solvent, usually miscible in all proportions. The solvent composition can be used to fine-tune the solvent quality at constant temperature.

2.2 Stepwise Fractionation Procedure

A classical method for fractionating a polydisperse polymer is to dissolve the polymer completely in a good solvent and then, progressively, to add small amounts of a poor solvent (nonsolvent). In the case of homopolymers, the high molecular weight polymer precipitates first. As more nonsolvent is added, progressively lower molecular weight polymer precipitates.

To obtain quantitative representation of fractionation, a model for the thermodynamic properties of the copolymer + solvent + nonsolvent system and the original two-dimensional distribution function are required. Rätzsch et al. [46] presented the application of continuous thermodynamics to successive homopolymer fractionation procedures based on solubility differences. This method is now applied to copolymer fractionation. The liquid–liquid equilibria (LLE) of polymer solutions forms the thermodynamic background for these procedures. The introduction of the precipitation rate (23) permits calculation of the distribution functions in the sol and gel phases of every fractionation step, i, according to:

$$\begin{aligned} X_i^{\mathrm{I}} W_i^{\mathrm{I}}(r,y) &= \frac{1 - K_i(r,y)}{1 - \phi_i} X_i^{\mathrm{F}} W_i^{\mathrm{F}}(r,y) \\ X_i^{\mathrm{II}} W_i^{\mathrm{II}}(r,y) &= \frac{K_i(r,y)}{\phi_i} X_i^{\mathrm{F}} W_i^{\mathrm{F}}(r,y). \end{aligned} \tag{31}$$

These relations provide the unknown distribution functions $W_i^{\mathrm{I}}(r,y)$ and $W_i^{\mathrm{II}}(r,y)$ directly.

Figure 3 presents the schemes for successive precipitation fractionation (SPF) and successive solution fractionation (SSF). In both cases, by lowering the temperature (or adding nonsolvent) a homogeneous polymer solution (called feed phase F) splits into two coexisting phases, a polymer-lean sol phase I and a polymer-rich gel phase II, which are then separated. In SPF (Fig. 3a), the polymer is isolated from phase II as fraction F1. Phase I directly forms the feed phase for the next fractionation step, etc.

In case of SSF (Fig. 3b), fraction F1 is obtained from phase I. Phase II is diluted by adding solvent up to the volume of the original feed phase, corresponding, to a very good approximation, to the same total amount of segments. This phase is used as a feed phase for step 2, etc. In the last fractionation step, the polymer of phase I in the case of SPF, or of phase II in the case of SSF, forms the final polymer fraction. All coexisting pairs of phase I and II are presumed to be in equilibrium. Hence, it is possible to apply all equations introduced above. To indicate the different separation steps 1,2,..., the corresponding number is added as a subscript.

According to the remarks made above, the total number of segments in SSF (Fig. 3b) is the same to a very good approximation in all feed phases. This leads to the following relations:

$$X_{i+1}^{\mathrm{F}} W_{i+1}^{\mathrm{F}}(r,y) = \phi_i X_i^{\mathrm{II}} W_i^{\mathrm{II}}(r,y) \quad r_{\mathrm{N},i+1}^{\mathrm{F}} = r_{\mathrm{N},i}^{\mathrm{II}} \quad y_{\mathrm{W},i+1}^{\mathrm{F}} = y_{\mathrm{W},i}^{\mathrm{II}}. \tag{32}$$

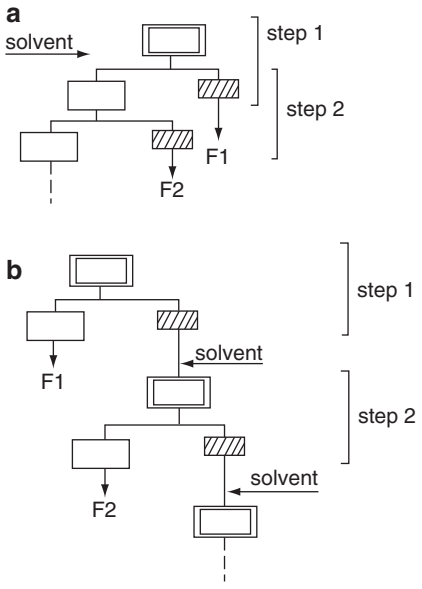

Fig. 3 Schemes of successive fractionation procedures: (**a**) successive precipitation fractionation (SPF), (**b**) successive solution fractionation (SSF). *F1* and *F2* are successive fractions

A constant feed volume can be achieved by adding solvent or solvent mixtures. The necessary amount is given by the amount separated with the polymer-lean phase:

$$n^*_{\mathrm{A},i} + n^*_{\mathrm{B},i} = n^{\mathrm{I}}_i = n^{\mathrm{F}}_i(1-\phi_i) \quad c_i = \frac{n^*_{\mathrm{A},i}}{n^{\mathrm{F}}_1}. \tag{33}$$

The quantity $n^*_{\mathrm{A},i}$ means the amount of segments of solvent A, which must be added at every fraction step i. This must be done to ensure that the amount of segment keeps constant at every fractionation step. The ratio c characterizes the composition of the solvent mixture added in every fractionation step. Working without a concentration gradient means that this ratio keeps constant during the fractionation procedure. The composition (Z) of the solvent mixture can be expressed by:

$$Z = \frac{X_{\mathrm{A}}}{1-X}. \tag{34}$$

The feed solvent composition for the fractionation step (i + 1) results from the mass balance (33):

$$Z^{\mathrm{F}}_{i+1} = \frac{Z^{\mathrm{II}}_i\left(1-X^{\mathrm{II}}_i\right)\phi_i + c_{i+1}}{1-X^{\mathrm{II}}_i\phi_i}. \tag{35}$$

From (32) as applied to fractionation step i, the distribution function of the i-th polymer fraction $W^I_i(r,y)$ can be derived in a direct and explicit form:

$$X^{\mathrm{II}}_i W^{\mathrm{II}}_i(r,y) = \frac{1-K_i(r,y)}{1-\phi_i}\prod_{j=1}^{i-1} K_j(r,y) X^{\mathrm{F}}_1 W^{\mathrm{F}}_1(r,y). \tag{36}$$

This relation corresponds to the fractionation scheme depicted in Fig. 3. In steps $j = 1, \ldots, i-1$, the polymer-rich phase II is taken to correspond to the occurrence of the factor $K_j(r, y)$ for $j = 1, \ldots, i-1$, according to (31). The polymer-lean phase I in step i is taken to correspond to the factor $(1 - K_i(r, y))/(1 - \phi_i)$, according to (31). The unknown quantities, $X^{\mathrm{II}}_j, Z^{\mathrm{II}}_j, r^{\mathrm{II}}_{\mathrm{N},j}, y^{\mathrm{II}}_{\mathrm{W},j}$, and ϕ_j (or T_j) for $j = 1, \ldots, i-1$ can be calculated successively with the help of the equations for LLE discussed above.

In SPF (Fig. 3a), phase I from step i is used directly as the feed phase for step i + 1. Hence, the following relations are valid:

$$W^{\mathrm{F}}_{i+1}(r,y) = W^{\mathrm{I}}_i(r,y) \qquad r^{\mathrm{F}}_{\mathrm{N},i+1} = r^{\mathrm{I}}_{\mathrm{N},i} \quad y^{\mathrm{F}}_{\mathrm{W},i+1} = y^{\mathrm{I}}_{\mathrm{W},i}. \tag{37}$$

According to the fractionation scheme, the amount of feed segments is not constant. In order to take this effect into account, the quantity λ_i is defined:

$$\lambda_i = \frac{n^{\mathrm{F}}_i}{n^{\mathrm{F}}_1}. \tag{38}$$

For $i = 1$, $\lambda_1 = 1$. In all other cases the material balance could be used to calculated λ_i:

$$\lambda_{i+1} = (1 - \phi_i)\lambda_i + c_{i+1} + d_{i+1} \quad d_i = \frac{n^*_{\mathrm{B},i}}{n^{\mathrm{F}}_1}. \tag{39}$$

The quantity $n^*_{\mathrm{B},i}$ means the amount of segments of solvent B, which must be added at every fraction step i. This must be done to ensure that the amount of segment keeps constant at every fractionation step. The quantity d_i describes the ratio of the added amount of solvent at every fractionation step and the amount of segment in the feed phase for the first fractionation step.

The polymer feed concentration for every fractionation step is given by:

$$X^{\mathrm{F}}_{i+1} = \frac{X^{\mathrm{I}}_i}{1 + \frac{c_{i+1}+d_{i+1}}{(1-\phi_i)\lambda_i}}. \tag{40}$$

If the fractionation is carried out only by lowering the temperature, then the polymer feed concentration in the step $i + 1$ is directly the polymer concentration of sol phase from step i. The composition of the solvent for the fractionation step $i + 1$ reads:

$$Z^{\mathrm{F}}_{i+1} = \frac{Z^{\mathrm{I}}_i\left(1 - X^{\mathrm{I}}_i\right)(1 - \phi_i)\lambda_i + c_{i+1}}{\left(1 - X^{\mathrm{I}}_i\right)(1 - \phi_i)\lambda_i + c_{i+1} + d_{i+1}}. \tag{41}$$

The fractions are taken from the gel phase. Therefore the distribution function in every fraction step i can be computed using:

$$X^{\mathrm{II}}_i W^{\mathrm{II}}_i(r, y) = \frac{K_i(r, y)}{\phi_i} \prod_{j=1}^{i-1} \frac{1 - K_j(r, y)}{1 - \phi_j} X^{\mathrm{F}}_1 W^{\mathrm{F}}_1(r, y). \tag{42}$$

This equation permits the direct and explicit calculation of the distribution function of the polymer fraction i from the distribution function of the original polymer. Again, the form of this relation corresponds to the fractionation scheme applied (Fig. 3a). In steps $j = 1, \ldots, i - 1$, the polymer-lean phase I is taken to correspond to the occurrence of the factor $(1 - K_j(r, y))/(1 - \phi_j)$ for $j = 1, \ldots, i - 1$, according to (31). In step i, the polymer-rich phase II is taken to correspond to the factor $K_i(r, y)/\phi_i$, according to (31). The unknown quantities, $X^{\mathrm{II}}_j, Z^{\mathrm{II}}_j, r^{\mathrm{II}}_{\mathrm{N},j}, y^{\mathrm{II}}_{\mathrm{W},j}$, and ϕ_j (or T_j) for $j = 1, \ldots, i - 1$ can be calculated successively with the help of the equations for LLE discussed above.

For example, SSF and SPF were applied to styrene–acrylonitrile copolymer in either toluene [62] or a mixture of methyl ethyl ketone and cyclohexane [63] as solvent. These types of fractionation are also called one-direction fractionations.

The cross-fractionation (CF) of copolymers suggested by Rosenthal and White [64] is a combination of several successive precipitation procedures and is also

called two-direction fractionation. The original copolymer is fractionated first in a precipitant–solvent system such that the mean content of A units of fractions, say, increases with an increase in their molecular weights. Then, every intermediate fraction is separated in another precipitant–solvent system, where the mean content of A units of fractions diminishes with an increase in their molecular weight. Rosenthal and White [64] assert that the final fractions separated in such a way are highly homogeneous both in molecular weight and in chemical composition.

For example, this method was carried out for various copolymers, namely styrene–methyl methacrylate copolymer [65–67], epoxide resins [68], styrene–acrylic acid copolymer [69], styrene–2-methoxyethyl methacrylate copolymer [70, 71], ethylene–α-olefin copolymer [72], partially modified dextran–ethyl carbonate copolymer [73], vinyl chloride–vinyl acetate copolymer [43], styrene–acrylonitrile copolymer [74], and styrene–butadiene copolymer [75].

The stepwise fractionation procedures (SSF and SPF) are one-direction fractionations and form the basis of cross-fractionation, where first the original polymer is fractionated in intermediate fractions using one solvent system and afterwards each intermediate fraction is further fractionated yielding the final fractions using another solvent system. There are four different possibilities for a fractionation strategy:

(a) SSF/SPF
(b) SSF/SSF
(c) SPF/SSF
(d) SPF/SPF

The theoretical framework introduced above can also be applied to cross-fractionation. This can be achieved by combination of the equations according to the selected fractionation strategy.

2.3 Baker–Williams Fractionation

Precipitation fractionation as developed by Baker and Williams [40] is one of the best-known column fractionation procedures. The fractionation is performed in a glass-bead-filled column with a temperature gradient down the column (Fig. 4). To start the fractionation, the total polymer is precipitated on the glass beads in a section at the entry of the column (or in a separate vessel). In a mixing vessel, a nonsolvent and a solvent are mixed to form a mixture with progressively increasing solvent power through continuous enrichment of the solvent. The polymer is dissolved by adding the solvent mixture. The resulting sol phase moves relatively slowly in the column, and the polymer in a given increment of the liquid sol stream becomes less soluble due to the temperature gradient and precipitates partially on the glass beads as a gel phase. The fractionation is achieved by the repeating exchange of polymer molecules between the stationary gel phase and the mobile sol phase. The superposition of a solvent + nonsolvent gradient and a temperature gradient leads to a very high separation efficiency.

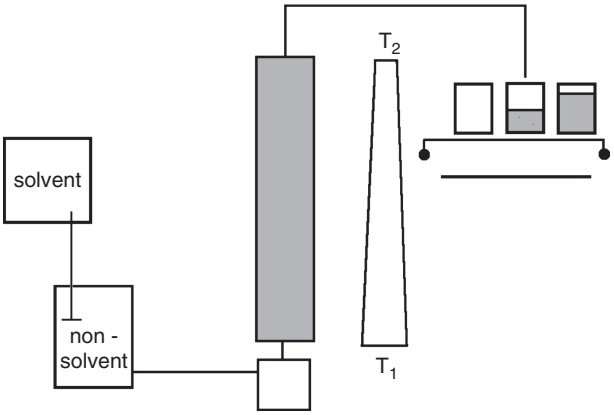

Fig. 4 Schematic of the Baker–Williams column, showing the temperature gradient down the column from higher temperature T_1 to lower temperature T_2

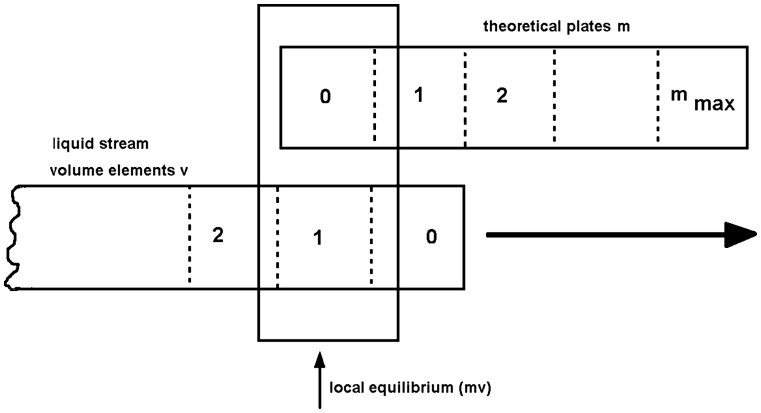

Fig. 5 Theoretical model of the Baker–Williams column

The theoretical treatment is based on a model subdividing the column into stages and the solution stream into parts with equal volumes. Hence, the column fractionation is considered as a combination of many local LLEs and treated in an analogous way as successive fractionation procedures. Rätzsch et al. [50] developed a model in order to simulate the fractionation of homopolymers according to the molar mass in a BW column by a number of local equilibria, similar to the model suggested by Smith [76] and by Mac Lean and White [77].

The column is subdivided into stages, labeled with m, starting with $m = 0$ (Fig. 5). The liquid stream is also subdivided into increments with equal volumes, labeled with v, starting with $v = 0$. At time zero the volume increment $v = 0$ fills stage $m = 0$; at time one the volume increment $v = 0$ occupies stage $m = 1$ and the

volume increment $v = 1$ occupies stage $m = 0$, etc. Each volume increment v at each stage m is considered to form liquid–liquid equilibrium (mv) between the sol phase I and the gel phase II.

The gel phase II, which is coated on the surface of the small glass beads, is stationary, i.e., it remains at the same stage m during the progress of time. However, the moving sol phase I always remains in the same volume increment v. Figure 5 depicts this situation. Starting the fractionation, the total polymer is assumed to be precipitated at stage $m = m_P = 0$ or to be distributed evenly among the $m_P + 1$ stages from $m = 0$ to $m = m_P$. The temperature gradient is expressed by [50]:

$$\begin{aligned} T_m &= T_0 & m < m_P \\ T_m &= T_0 - (m - m_P)\Delta T & m > m_P. \end{aligned} \tag{43}$$

Here T_m is the temperature of stage m and ΔT is the constant temperature difference between neighboring stages. The segment fraction Z of the solvent in the solvent + nonsolvent mixture supplied to the entry (*) of the column, $Z^*_{v,0}$, is assumed to be given by [50]:

$$Z^*_{0,v} = Z^*_{0,0} + Z^*\left(1 - \exp\left(-\frac{v}{v^*}\right)\right), \tag{44}$$

where $Z^*_{0,0}$, ΔZ^*, and v^* are the parameters of this function. The polymer fractions are obtained from the sol phase I of the last stage.

The suggested theory is based on the model described above, which subdivides the column fractionation procedure into many local phase equilibria (Fig. 5). In this way, the phase equilibrium relation presented above can be applied. The considered volume increment v and the considered column stage m are indicated as subscripts of the corresponding quantities. The feed quantities for every LLE can be calculated by applying the above model. However, it has to be taken into account that the feed phase is not a homogenous phase. The feed phase $(m + 1, v + 1)^F$ is the sum of the mobile phase $(m,v + 1)^I$ and the stationary phase $(m + 1, v)^{II}$. After equilibrium, the sol phase $(m + 1, v + 1)^I$ and the gel phase $(m + 1, v + 1)^{II}$ are formed. Therefore, the mass balance for the copolymer reads:

$$\begin{aligned} &\eta\left[\lambda(1-\phi)X^I W^I(r,y)\right]_{m,v+1} + \tau\left[\lambda\phi X^{II} W^{II}(r,y)\right]_{m+1,v} + \theta\left[X^F W^F(r,y)\right]_{0,0} \\ &\quad = \left[\lambda X^F W^F(r,y)\right]_{m+1,v+1}, \end{aligned} \tag{45}$$

where the parameters η, τ, and θ are given by:

$$\begin{aligned} &\eta = 0 \quad \text{for} \quad m+1=0 \quad \eta = 1 \quad \text{for} \quad m+1>0 \\ &\tau = 0 \quad \text{for} \quad v+1=0 \quad \tau = 1 \quad \text{for} \quad v+1>0 \\ &\theta = 0 \quad \text{for} \quad m+1>m_P \; \theta = 0 \quad \text{for} \quad m+1<m_P \quad \text{and} \quad v+1=m. \end{aligned} \tag{46}$$

The quantity $\lambda_{m,v}$ in (45) measures the ratio of the segments in the feed phase $(m,v)^{\mathrm{F}}$ and the feed phase $(0,0)^{\mathrm{F}}$. At stage $m = 0$ the condition:

$$\lambda_{0,v} = 1 \tag{47}$$

is realized by the amount of solvent mixture added. In all other cases, λ_{mv} follows from the phases combined, leading to:

$$\left[\lambda X^{\mathrm{F}}\right]_{m+1,v+1} = \eta\left[\lambda(1-\phi)X^{\mathrm{I}}\right]_{m,v+1} + \tau\left[\lambda\phi X^{\mathrm{II}}\right]_{m+1,v} + \theta X^{\mathrm{F}}_{0,0}. \tag{48}$$

The ratio of the solvent in the solvent + nonsolvent mixture in the corresponding feed phase is given by:

$$\begin{aligned}\left[\lambda Z^{\mathrm{F}}\left(1-X^{\mathrm{F}}\right)\right]_{m+1,v+1} = {} & \eta\left[\lambda(1-\phi)Z^{\mathrm{I}}\left(1-X^{\mathrm{I}}\right)\right]_{m,v+1} \\ & + \tau\left[\lambda\phi Z^{\mathrm{II}}\left(1-X^{\mathrm{II}}\right)\right]_{m+1,v} + \sigma\left(1-\phi_{0,v}\right)Z^{*}_{0,v+1}\end{aligned} \tag{49}$$

with:

$$\sigma = 1 \quad \text{for} \quad m+1 = 0 \qquad\qquad \sigma = 0 \quad \text{for} \quad m+1 > 0. \tag{50}$$

The quantity $Z^{*}_{0,v+1}$ can be calculated using (44). The combination of (31), as applied to the considered equilibrium, and of (45) interrelates the polymer distributions in the feeds of neighboring equilibria:

$$\begin{aligned}\left[\lambda X^{\mathrm{F}}W^{\mathrm{F}}(r,y)\right]_{m+1,v+1} = {} & \left[\lambda(1-K(r,y))X^{\mathrm{F}}W^{\mathrm{F}}(r,y)\right]_{m+1,v} \\ & + \left[\lambda K(r,y)X^{\mathrm{F}}W^{\mathrm{F}}(r,y)\right]_{m,v+1}.\end{aligned} \tag{51}$$

This equation permits the direct and explicit calculation of the various copolymer distribution functions $W^{\mathrm{F}}_{m,v}(r,y)$ from the distribution function $W^{\mathrm{F}}_{0,0}(r,y)$.

2.4 Continuous Polymer Fractionation

The production of sufficient amounts of narrowly distributed polymer samples, which cannot by synthesized with narrow molecular weight distribution, has been too laborious, except for special cases like the investigation of dilute solutions, for which only small polymer samples are required. This situation was strongly improved by the development of a new technique. Wolf et al. [78] suggested a continuous polymer fractionation method for homopolymers that allows fractions on the 100 g scale.

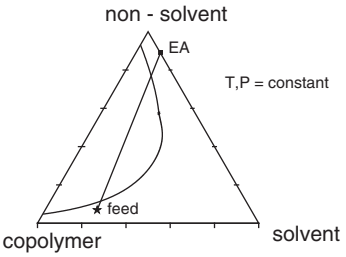

Fig. 6 Scheme of the CPF in a Gibbs phase triangle

The polymer to be fractionated is dissolved in a solvent + nonsolvent mixture, and this solution (feed) is extracted continuously by a second liquid (extracting agent, EA), which contains the same solvent components as the feed (Fig. 6). The fractionation can be performed with a pulsed counter-current extraction apparatus. Fractionation is achieved by the fact that the molecules are distributed over the counter-current phases according to their chain length. The feed leaves the column as gel and the EA as sol.

The solvent components in the feed and in the EA are chosen such that (a) the entire system formed by the starting polymer and the solvent components exhibits a miscibility gap at the temperature of operation; (b) that, in the Gibb's phase triangle, the composition of the feed corresponds to a point outside of this miscibility gap; and (c) that the EA is composed in such a way that the straight line drawn between feed and EA (working line) intersects the miscibility gap (Fig. 6).

The ratio of flows of feed and EA is chosen such that the working point (average composition of the total content of the apparatus under stationary operating conditions) is located at higher polymer concentration than the intersection of the working line with the branch of low polymer concentration of the demixing curve (Fig. 6). As the original feed comes into first contact with the already polymer-loaded phase originating from the pure EA and moving in the opposite direction, the most easily soluble low molecular weight polymer molecules will be transferred to this dilute phase, which in turn segregates its most sparingly soluble high molecular weight material to the more concentrated phase in order to achieve phase equilibrium. By providing for a high number of such equilibria in the course of the counter-current extraction (proportional to the number of bottoms when a sieve-bottom column is used), the polymer contained in the more concentrated phase will have lost practically all the low molecular weight material contained in the original sample up to a certain characteristic chain length, when it leaves the apparatus after a final extraction by the pure EA. In an analogous manner, the molecular weight distribution of the polymer contained in the less-concentrated phase will narrow as the counter-current extraction proceeds. The feed leaves the column as gel and the EA as sol. The distribution of the polymer on the sol and gel phases can be regulated by the solvent + nonsolvent ratio in the EA and by the ratio of the flux rates of feed and EA. The fractionation efficiency can be increased by additional measures, like pulsation,

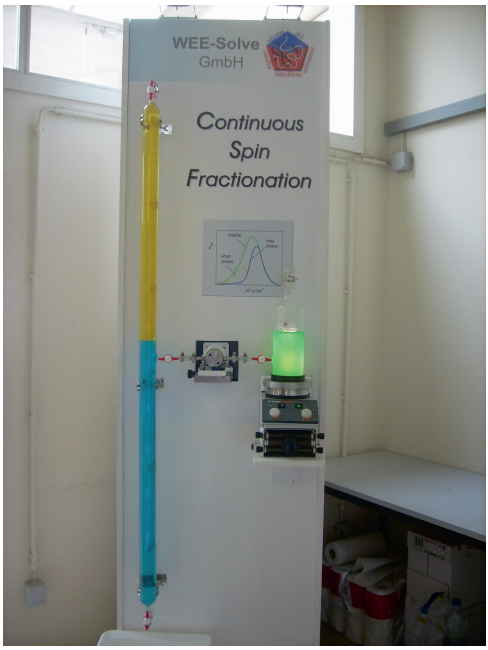

Fig. 7 Photograph of the CSF apparatus

which leads to a higher dispersion of the phases. If the desired separation cannot be obtained in one step, the gel can directly be used as feed, whereas in the case of the sol the polymer must be precipitated before it can be used as feed again. This method was applied to numerous polymers, i.e., polyethylene [79], hydroxyethyl starch [80], polycarbonate [81], polyacrylacid [82], and polyisobutylene [83, 84].

This fractionation method was further developed in 2002 [85, 86] by employing a spinning nozzle (Fig. 7). The new method is called continuous spin fractionation (CSF). The feed phase is pressed through a spinning nozzle to jet threads of the viscous polymer solution, which disintegrate rapidly because of the Rayleigh instability. In this manner, one obtains a large amount of tiny droplets in the desired EA. The droplets with a large ratio of surface to volume facilitate the escape of short chains from entanglements of higher macromolecules due to the short distance of transport. For that reason, CSF not only eliminated the damming-back problem of CPF, but can also be operated successfully at considerably higher polymer concentrations.

The CPF was applied also to copolymers [87, 88]. For example, polycarbonate–siloxane (PC–Si) copolymers are characterized by an outstanding thermal stability, good weathering properties, excellent flame retardancy, and high impact resistance at low temperature [87]. PC–Si materials are used in numerous applications including windows, roofing, contact lenses, and gas-permeable membranes. Depending on the siloxane-block length and domain size, the copolymers are transparent,

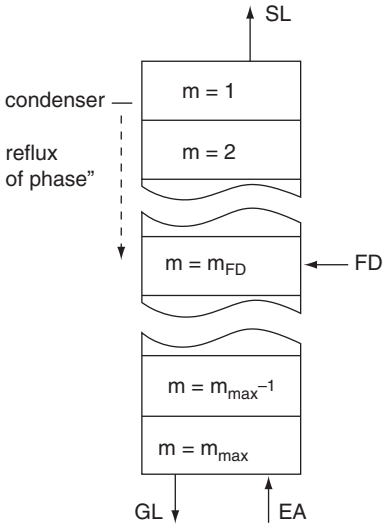

Fig. 8 Model of the improved CPF column. *SL* sol, *GL* gel

translucent, or opaque [89]. The CPF allows fractionation according to the chemical composition and according to the molecular weight and, hence, the tailoring of the copolymer for a certain application purpose.

Rätzsch et al. [48, 49] proposed a theoretical treatment of the CPF similar to that of the BW fractionation. The CPF column is divided into a number of stages m (Fig. 8). The EA enters the column at stage $m = m_{\mathrm{Max}}$ and leaves it as sol at stage $m = 1$. The stationary state is calculated by repeating calculation of stages $m = 1, \ldots, m_{\mathrm{Max}}$. At start ($i = 0$), the column is filled with EA. For the first set of equilibria ($i = 1$), a certain amount of feed (FD) is added at stage $m = 1$, and the related phase II is transferred downwards to the next stage $m = 2$, filled with EA. When phase II has left the column at m_{Max} as the first, nonstationary gel phase, all phases I are shifted by one stage upwards, and stage m_{Max} is filled with pure EA again. The calculation is repeated for $i = 2$ and $m = 1, \ldots, m_{\mathrm{Max}}$ etc. The stationary state is reached when the results for i and $i - 1$ no longer change systematically.

Using this simulation procedure, some improvements could be suggested [48]. The pulsating sieve-bottom column was replaced by a non-pulsating column filled with glass beads. In this manner, the number of theoretical plates could be raised considerably. A further improvement of the fractionation efficiency results from the reflux of part of the polymer contained in the sol phase. In practice, this situation was realized by putting a condenser on the top of the column and introducing the feed somewhere near of the upper third of the column (Fig. 8). These suggestions were verified experimentally using the system dichloromethane/diethylene glycol/ bisphenol-A polycarbonate [48]. Except for the lowest molecular weight fraction, one obtains nonuniformities on the order of 0.1.

For conventional CPF, where the FD is introduced on the top, the calculation of stationary states starts ($i = 0$) with the entire column filled with EA. For the first set of equilibria ($i = 1$), a certain amount of FD, determined by the chosen working conditions of CPF, is introduced at m_{FD} (Fig. 6). After the equilibrium has been calculated for this plate, phase II is transferred downwards to the next theoretical plate filled with EA and a new equilibrium on plate $m_{\mathrm{FD}} + 1$ is determined. This procedure is repeated until phase II leaves the column as the first (nonstationary) gel phase at m_{Max}. In preparation of the next step of calculation ($i = 2$), all phases I are shifted by one plate upwards, i.e., from m to $m - 1$ so that the first (nonstationary) sol phase leaves the column at m_{FD}. Furthermore, plate m_{Max} is again filled with pure EA. After the addition of another portion of FD, the determination of the next set of equilibria ($i = 2$) proceeds as described for $i = 1$. This treatment is repeated until the stationary state is reached, which means that the results for i and $i - 1$ no longer change systematically.

The mass balance for the polymer transfer is formulated in terms of $w(r, y)$, the extensive segment-molar distributions obtained by multiplying $W(r, y)$ by the overall amount of polymer segments present in a given system. For the transfer between neighboring phases, the following relation can be formulated:

$$w^{\mathrm{I}}_{m+1,i-1}(r,y) + w^{\mathrm{II}}_{m-1,i}(r,y) = w^{\mathrm{F}}_{m,i}(r,y). \tag{52}$$

For $i = 1$, the first term becomes zero and for $m = m_{\mathrm{FD}}$ the additional term $w^{\mathrm{FD}}_{i}(r,y)$ has to be added on the left side of the equation. For $m = m_{\mathrm{Max}}$ the first and for $m = 1$ the second term vanish. In the case of conventional CPF, m_{FD} is equal to unity. For the mass balance for the subdivision of the polymer among the phases coexisting on one theoretical plate, the corresponding equation reads:

$$w^{\mathrm{F}}_{m,i}(r,y) = w^{\mathrm{I}}_{m,i}(r,y) + w^{\mathrm{II}}_{m,i}(r,y). \tag{53}$$

In the calculation outlined above, the amount of segments contained in a theoretical plate changes with i within the nonstationary phase. For this reason, a quantity ε is introduced as the ratio of the overall amount of segments present in plate m during step i and during step zero. From the material balance between adjacent theoretical plates, one obtains the following relation:

$$\varepsilon_{m,i} = [\varepsilon(1-\phi)]_{m+1,i-1} + [\varepsilon\phi]_{m-1,i} \tag{54}$$

with the limiting conditions $\varepsilon_{m,0} = 0$ for $m = 1$ up to $m = m_{\mathrm{FD}} - 1$ (improved CPF), and $\varepsilon_{m,0} = 1$ for $m = m_{\mathrm{FD}}$ to $m = m_{\mathrm{Max}}$. For $m = m_{\mathrm{FD}}$, the extra term $\varepsilon_{\mathrm{FD}}$ (which is determined by the amount of segments added with the feed, normalized to the amount of EA present on this plate for $i = 0$) has to be added on the right side of

the equation. For $m = m_{\mathrm{Max}}$ and $i > 0$, the first term becomes unity and for $m = 1$ the second term vanishes. To obtain the material balances for the polymer, (52) and (53), in terms of the normalized distribution function $W(r, y)$, one divides these relations by the total amount of segments in a plate at $i = 0$. This leads to:

$$\left[\varepsilon(1-\phi)X^{\mathrm{I}}W^{\mathrm{I}}(r,y)\right]_{m+1,i-1} + \left[\varepsilon\phi X^{\mathrm{II}}W^{\mathrm{II}}(r,y)\right]_{m-1,i} = \left[\varepsilon X^{\mathrm{F}}W^{\mathrm{F}}(r,y)\right]_{m,i}, \quad (55)$$

where the special cases discussed in the context of (52) apply analogously, and to:

$$\left[X^{\mathrm{F}}W^{\mathrm{F}}(r,y)\right]_{m,i} = \left[(1-\phi)X^{\mathrm{I}}W^{\mathrm{I}}(r,y)\right]_{m,i} + \left[\phi X^{\mathrm{II}}W^{\mathrm{II}}(r,y)\right]_{m,i}. \quad (56)$$

As described above, the stationary state is approached by the stepwise calculation of the composition of the coexisting phase using the equation given in Sect. 3.1, where the information concerning all previous states is required in the actual calculation.

3 Results and Discussion

The suggested fractionation theory is based on the LLE of a copolymer solution; therefore, first the calculation procedure related to the LLE is discussed. Additionally, the calculation results are compared with experimental LLE data for ethylene vinyl acetate copolymer (EVA) in methyl acetate taken from literature [90].

Subsequently, the theory is applied to stepwise fractionation using the cross-fractionation procedure. After some model calculations to study the influence of different operative fractionation parameters on the fractionation efficiency, the theoretical results will be again compared with experimental data for the styrene–butadiene copolymer system in two different solvent systems, namely cyclohexane + isooctane and benzene + methyl ethyl ketone [75].

Finally, the theoretical framework is applied to the simulation of column fractionation according two different methods (BW fractionation and CPF). In both types of fractionation, the influence of operative conditions on the fractionation effect with respect to the molecular weight and the chemical composition is investigated. Because of the lack of experimental data, no comparison with experiments was possible.

3.1 Liquid–Liquid Phase Equilibrium of Copolymer Solutions

The copolymer fractionation aims at the production of fractions having a distribution as narrow as possible. For this reason, this chapter focuses on the distributions in the sol and gel phases. Before any calculations can be carried out, the model parameters must be chosen. The model parameters can be divided into:

(a) Parameters describing the feed polymer
(b) Parameters describing the selected solvent + nonsolvent system
(c) Parameters describing the operative conditions

The feed polymer can be characterized by a two-dimensional distribution function, (15) or (16). Typical values for parameters of these distribution functions are:

$$r_N = 100 \quad k = 1 \quad \varepsilon = 0.25 \quad y_W = 0.5 \quad \alpha = \beta = 4. \tag{57}$$

Setting $\alpha = \beta$ in (16) means that the distribution function with respect to the chemical heterogeneity is symmetrical. The parameters describing the selected solvent + nonsolvent system occur in the G^E model [i.e., (5)]. For the model calculation, the following parameter were chosen:

$$\begin{aligned} &r_A = 1 \quad \chi_{AP} = 150\ \text{K} \quad p_A = 0 \quad \gamma_A = 0.5 \\ &r_B = 1 \quad \chi_{BP} = 250\ \text{K} \quad p_B = 0 \quad \gamma_B = 1 \\ &\chi_{AB} = 500\ \text{K}. \end{aligned} \tag{58}$$

The low-molecular weight component A should act as solvent. The parameter χ_{AP} is selected in a way that no demixing with the copolymer occur. The low molecular weight component B takes over the role of the nonsolvent and, hence, the parameter χ_{BP} leads to a miscibility gap with the polymer. The selected operative conditions are:

$$X^F = 0.01 \quad Z^F = 0.2 \quad T = 350\ \text{K}. \tag{59}$$

The asymmetry of the distribution with respect to the chemical composition has a large impact on the phase equilibria of copolymers [6]. First the influence of the feed distribution (16), especially the symmetry, is studied. At constant mass-average chemical composition, the maxima of the distribution according to the chemical composition are shifted to higher values if the distribution become unsymmetric ($\alpha = 4$ and $\beta = 2$). The distribution $W(100, y)$ in the sol and gel phases are plotted in Fig. 9. The symmetry of the feed copolymer has a large impact on the theoretical fractionation results. Caused by the shift of the maxima in the feed distribution, the maxima in the fractions shift also to higher values. Moreover, in the case of a symmetric feed distribution (solid lines in Fig. 9) more polymer molecules will be in the sol phase in comparison with an unsymmetric feed distribution (broken lines in Fig. 9). If a modified version of (16) is used, namely ignoring the polydispersity with respect to the molecular weight, the ratio between the amounts of sol and gel phases does not change if the parameter β is changed from $\beta = 4$ (symmetrical case) to $\beta = 2$ (unsymmetrical case). This finding indicates the complex interactions of both polydispersities.

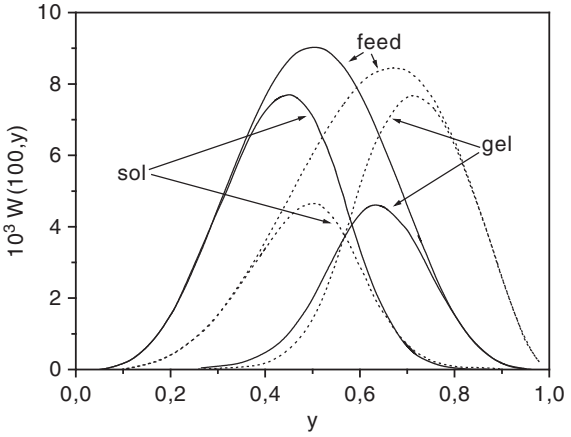

Fig. 9 Distribution of chemical composition at $r = 100$ in the sol and gel phases, where the feed distribution is given by (16): *solid lines* $\alpha = \beta = 4$; *broken lines* $\alpha = 4$, $\beta = 2$

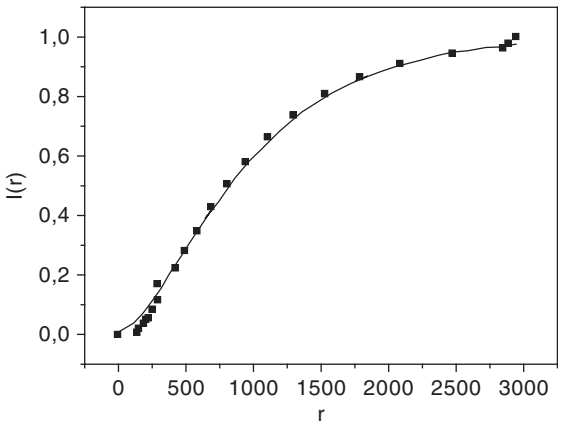

Fig. 10 Fit (*solid line*) of the experimental feed distribution [90] (*squares*) of EVA copolymer

In order to verify the present theoretical framework, the calculation results are compared with experimental data. Schirutschke [90] carried out phase equilibrium experiments (critical point, cloud-point curves) of the system EVA + methyl acetate. The distribution of the copolymer was measured using the successive fractionation procedure and determination of the number-average molecular weight of every obtained fraction. Using this data, the integral distribution function, $I(r)$, can be constructed (Fig. 10) and the parameter of the distribution function with respect to the molecular weight can be estimated. Fitting of the data given in Fig. 10 results in $r_N = 429$ and $k = 0.758$, where the ethylene monomer unit was chosen as standard. The mass-average chemical composition $y_W = 0.375$ was measured

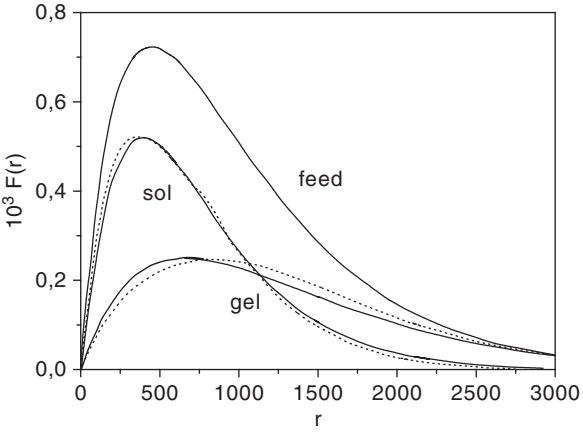

Fig. 11 Comparison of experimental [90] (*solid line*) and calculated (*broken line*) fractionation for EVA in methyl acetate

using elementary analysis. The broadness of the distribution, ε, was estimated using the Stockmayer theory [56], yielding $\varepsilon = 0.25$. The parameters occurring in the G^{E} model (5) were chosen as:

$$r_{\mathrm{A}} = 2.08 \quad \chi_{\mathrm{AP}} = 80.75\ \mathrm{K} \quad p_{\mathrm{A}} = 0.1 \quad \gamma_{\mathrm{A}} = 0.3. \tag{60}$$

Unfortunately, Schirutschke [90] did not give any information about the chemical polydispersity in the experimentally obtained fraction. For this reason, the comparison between the experiment and the modeling results is limited to the fractionation according to the molecular weight. In Fig. 11, the function $F(r)$, which is defined as:

$$F(r) = \int_0^1 W(r, y)\mathrm{d}y \tag{61}$$

is compared with the experimental data [90], where the experiment was performed at 303.15 K. From Fig. 11, it can be concluded that the proposed theoretical framework is able to describe the polymer distribution in the coexisting phases. Moreover, this comparison also shows the large impact on the LLE of the chemical heterogeneity, even if the broadness of this function is only small.

3.2 Stepwise Fractionation Procedure

Cross-fractionation as a mean of evaluating the molecular weight and chemical-composition distribution of heterogeneous copolymer is composed of two steps.

The sample is first fractionated into intermediate fractions in one solvent + nonsolvent system (solvent mixture 1). This is followed by further fractionation of these intermediate fractions by another solvent + nonsolvent system (solvent mixture 2).

3.2.1 Influence of the Fractionation Strategy

Using the SSF (Fig. 3b) and SPF (Fig. 3a) techniques, copolymers can be fractionated using the cross-fractionation method by combining the two basic types for fractionation in solvent mixtures 1 and 2. This situation results in four different fractionation strategies: SSF/SPF, SPF/SSF, SPF/SPF, and SSF/SSF, where the solvent mixture is changed for the fractionation of the intermediate fractions. The first question arising in this situation is which strategy should be used in order to optimize the fractionation efficiency. To answer this question, calculation of all four strategies were performed.

In these simulations, it was assumed that both solvent mixtures are made only from one solvent. The applied parameters in the G^{E} model (5) for the solvent 1 are:

$$r_{\mathrm{A}} = 1 \quad \chi_{\mathrm{AP}} = 250\ \mathrm{K} \quad p_{\mathrm{A}} = 0 \quad \gamma_{\mathrm{A}} = 1 \tag{62}$$

and for the solvent 2:

$$r_{\mathrm{A}} = 1 \quad \chi_{\mathrm{AP}} = 220\ \mathrm{K} \quad p_{\mathrm{A}} = 0 \quad \gamma_{\mathrm{A}} = 0.5. \tag{63}$$

During the simulation, the original polymer was fractionated into five intermediate fractions using the solvent 1 (62), whereas every intermediate fraction was further divided into five final fractions using the solvent 2 (63). The temperatures for every fractionation step were selected in such a way that in every fraction the same amounts of polymer were present. The polymer feed concentration, expressed in segment fractions, was 0.01. Figure 12 depicts the calculated mass-average chemical composition of every fraction using the four different fractionation strategies. The fractions numbered 10–15 represent the chemical composition of the final fractions, obtained from the first intermediate fraction. The fractions numbered with 20–25 represent the chemical composition of the final fractions, obtained from the second intermediate fraction, and so on. If the fractionation in solvent 1 is carried out using the SPF mechanism (circles and crosses in Fig. 12), the mass-average chemical composition of the intermediate fractions decrease with the number of the fraction. Under this circumstance the fractionation in the solvent 2 can be performed using SPF (circles in Fig. 12) or SSF (crosses in Fig. 12). Except for the final fractions from the first intermediate fraction, where the SPF mechanism leads to a decrease in the y_{W} values and the SSF to increasing values for this quantity, in all other final fractions the y_{W} value increases by SSF and decreases by SPF. If the fractionation in the solvent 1 is carried out using the SSF mechanism

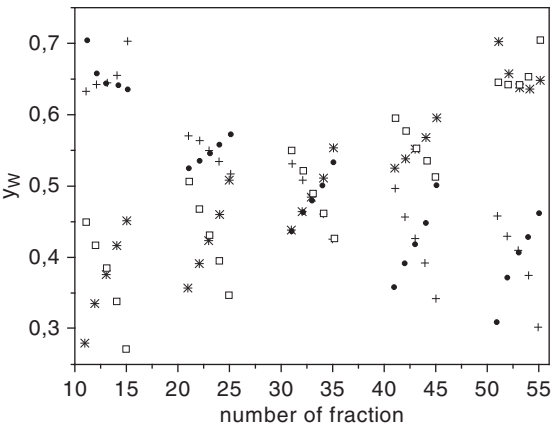

Fig. 12 Mass-average chemical composition for every fraction obtained by cross-fractionation using different fractionation strategies: *circles* SPF/SPF, *crosses* SPF/SSF, *stars* SSF/SPF, and *squares* SSF/SSF

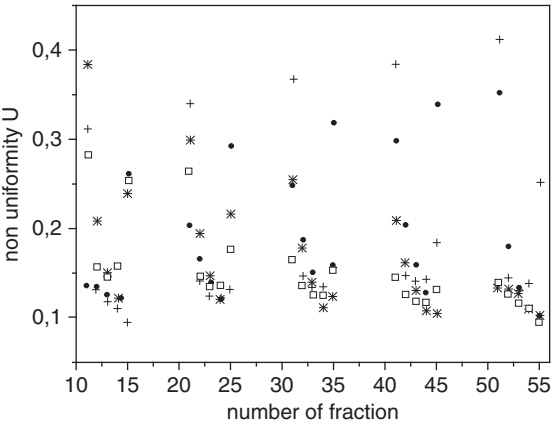

Fig. 13 Nonuniformity for every fraction obtained by cross-fractionation using different fractionation strategies: *circles* SPF/SPF, *crosses* SPF/SSF, *stars* SSF/SPF, and *squares* SSF/SSF

(stars and squares in Fig. 12), the mass-average chemical composition of the intermediate fractions increases with the number of fraction. All fractions, except the fractions obtained from the last intermediate fractions, show a similar behavior. If the fractionation of the intermediate fractions in solvent 2 is carried out using the SPF mechanism (stars in Fig. 12), the mass-average chemical composition increases with the number of fraction, whereas the chemical composition decreases if the second fractionations in the solvent 2 is performed with the SSF method (squares in Fig. 12). Using the data in Fig. 12, it can be concluded the SSF/SSF strategy leads to the fractionation having the highest effectivity in terms of fractionation according to the chemical composition.

In Fig. 13, the fractionation results with respect to the molecular weight are plotted in terms of the nonuniformity of the obtained fractions. Independently of the fractionation strategy applied, all obtained final fractions have a much smaller

nonuniformity than the original polymer. Using the SPF/SPF method (circles in Fig. 13), the last fraction of every intermediate fraction always shows the highest value for the nonuniformity. With increasing number of the intermediate fraction this effects is more pronounced. Applying the SPF/SSF mechanism (crosses in Fig. 13), the highest nonuniformity is always observed in the first final fraction of every intermediate fraction, similar to the results for the SSF/SPF mechanism (stars in Fig. 13). Similar to the results discussed above, the SSF/SSF (squares in Fig. 13) leads to the most effective fractionation, also according to the molecular weight, and hence this method can be recommended for the cross-fractionation.

3.2.2 Influence of the Solvent Mixture

The fractionation based on the LLE and the LLE depends strongly on the interactions between the molecules present in the system. In connection with the effectivity of copolymer fractionation, it must be investigated by how much both solvents used in the cross-fractionation procedure should differ in terms of solution power for the copolymer. The quality of solvent can be expressed by the interaction parameter occurring in the G^{E} model (5). Calculations were done using two different parameter sets, representing a large difference between the interactions of the solvents 1 and 2 with the copolymer:

$$\begin{aligned} \chi_{\mathrm{AP}} &= 250\ \mathrm{K} \quad p_{\mathrm{A}} = 0 \quad \gamma_{\mathrm{A}} = 1 \\ \chi_{\mathrm{BP}} &= 350\ \mathrm{K} \quad p_{\mathrm{B}} = 0 \quad \gamma_{\mathrm{B}} = 0.15 \end{aligned} \tag{64}$$

and representing only a small difference in these parameters:

$$\begin{aligned} \chi_{\mathrm{AP}} &= 250\ \mathrm{K} \quad p_{\mathrm{A}} = 0 \quad \gamma_{\mathrm{A}} = 1 \\ \chi_{\mathrm{BP}} &= 220\ \mathrm{K} \quad p_{\mathrm{B}} = 0 \quad \gamma_{\mathrm{B}} = 0.5. \end{aligned} \tag{65}$$

The calculation results are depicted in Fig. 14 in terms of the Breitenbach–Wolf plot with respect to the segment number (Fig. 14a) and with respect to the chemical composition (Fig. 14b). The fractionation effect can be analyzed by the slope of the Breitenbach–Wolf plot. If the two solvents differ strongly, the Breitenbach–Wolf plot with respect to the segment number has a larger slope meaning a higher fractionation effect (Fig. 14a). However, analyzing the data given in Fig. 14b for the fractionation effect according to the chemical composition, the converse can be concluded. The reason for this finding is the difference in the parameter γ_{A} for the solvent 2. Whereas the Flory–Huggins parameter χ_{AP} has an impact on both fractionations types, the parameter γ_{A} only has an impact on the fractionation with respect to the chemical heterogeneity. For practical purposes, the χ_{AP} parameters should have a large difference in order to make sure an effective fractionation according the molecular mass, and the γ_{A} parameter should be always quite

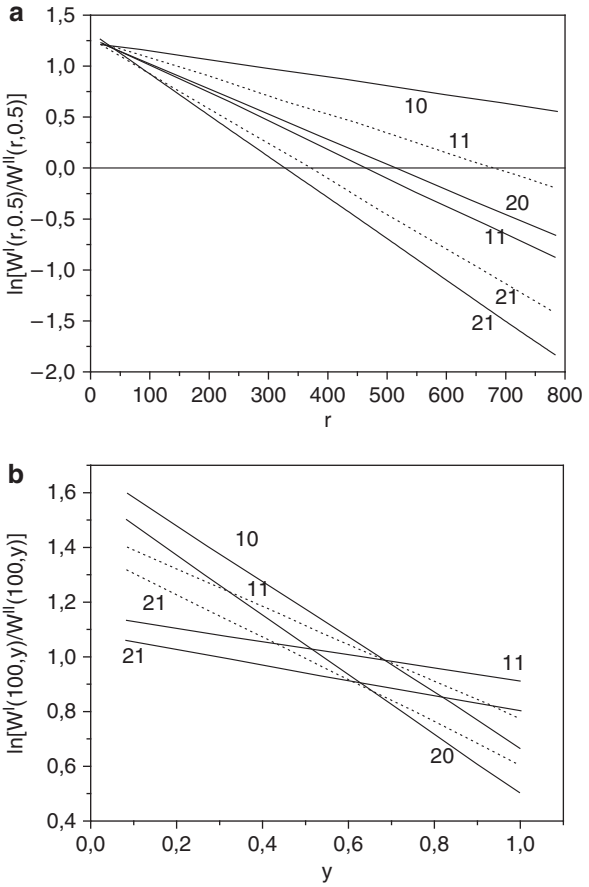

Fig. 14 Breitenbach–Wolf plot with respect to the segment number (**a**) and with respect to the chemical composition (**b**). The *numbers* indicate the final fraction number. The *solid lines* are calculated using the parameter given in (64) and the *broken lines* are obtained using the parameters of (65)

large in order to ensure an effective fractionation according to the chemical composition.

For the production of the intermediate, as for the production of the final fraction, a temperature gradient must also be established. This gradient can be chosen to be linear or nonlinear. The nonlinear temperature gradient is selected in such a way that every final fraction contains the same amount of copolymer segments. The fractionation results are demonstrated in Fig. 15, where the distribution functions with respect to the segment number for the fraction obtained from the third intermediate fractions are shown. It can be recognized clearly that the second approach of keeping the amount of polymer in every final fraction constant is the

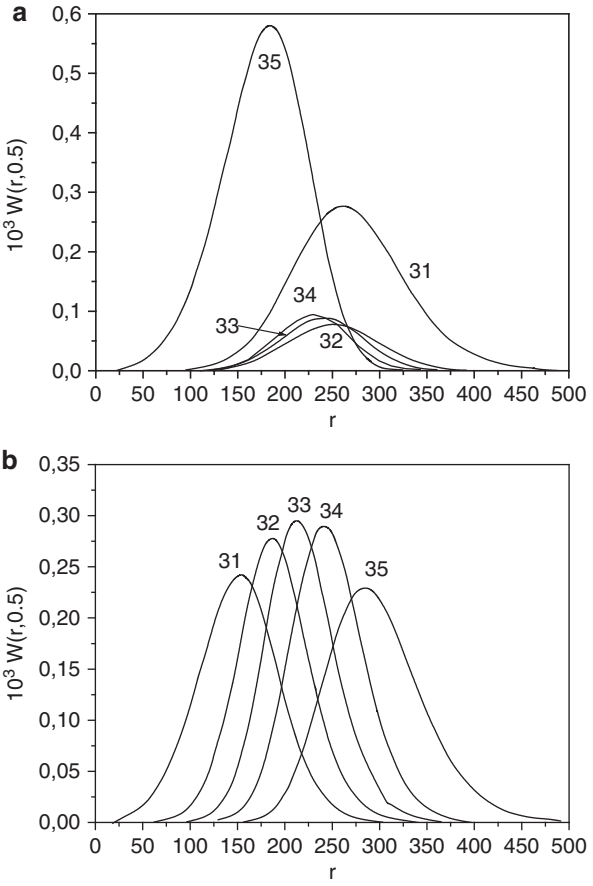

Fig. 15 Influence of the temperature gradient on the fractionation according the segment number for different temperature gradients: (**a**) linear temperature gradient, (**b**) nonlinear temperature gradient. The *numbers* indicate the final fraction number

better choice, because the obtained distribution functions are narrower and the overlapping of the distribution functions is less pronounced.

Additionally, the same calculations were performed in order to investigate whether a more effective fractionation could be achieved using solvent mixtures such as solvent 1 and solvent 2. This situation allows, from the theoretical point of view, a combination of the solvent gradient and a temperature gradient. However, the calculation results make it clear that no improvement could be seen if both gradients were applied. The most important criterion for effective fractionation was equal amounts of polymer in every final fraction. This criterion can be achieved by solvent gradient or temperature gradient, or both. For the solution of a practical fractionation problem, the search for a suitable solvent combination, in particular if

solvent mixtures are to be used, is a very time-consuming task. This task can be abbreviated if only two solvents and not two solvent mixtures are needed. The criterion of equal amounts of polymer in every final fraction can be fulfilled by a suitable nonlinear temperature gradient.

3.2.3 Cross-Fractionation

Teramachi and Kato [75] performed experimentally a cross-fractionation according the SPF/SPF mechanism and two SPFs in different solvent systems of styrene–butadiene copolymer. The copolymer was an industrial product that was polymerized to about 100% conversion with *n*-butyl lithium. Teramachi and Kato used two solvent systems, namely solvent mixture 1 (cyclohexane + isooctane) and solvent mixture 2 (benzene and methyl ethyl ketone). During all experimental fractionations, the temperature was kept constant at 25°C. In cross-fractionation, the sample was first fractionated into four intermediate fractions in solvent mixture 2 and then each intermediate fraction was fractionated into five fractions in solvent mixture 1. The SPF yield in solvent mixture 1 was 13 fractions, and ten fractions in solvent mixture 2. The original copolymer, as well all obtained fractions, were analyzed using a membrane osmometer for the determination of the number-average molecular weight, and refractive index measurement for the determination of the average chemical composition. In the experiments [75], it was found that the analysis of both one-direction fractionations using different solvent systems led to identical chemical composition distributions for the original polymer; however, both results are not always true. The analysis of the cross-fractionation data gave a broader distribution curve of the chemical heterogeneity and the molecular weight than the one-direction fractionations. The component with low styrene contents (lower than 17 mol%) could only be found by cross-fractionation.

These experimental data give us the possibility to verify the present theory with experiments. From the analysis of the original polymer, two parameters of the Stockmayer distribution function (15), namely $r_N = 884.9$ and $y_W = 0.2799$, are available. The conversion in the polymerization reaction was close to 100% and hence the Stockmayer theory [56] cannot be applied to estimate ε. The values for $\varepsilon = 1.9$ and $k = 2$ were estimated by fitting them to the integral distribution of the original polymer. Next, the parameter of the G^E model (5) must be estimated. Unfortunately, Teramachi and Kato [75] gave no information about the concentration gradient used during the fractionation procedure. Model calculations indicated that the fractionation results can be achieved by a solvent mixture or by a pure solvent. In order to minimize the number of adjustable parameters, both solvent mixtures were simulated by only one "mean" solvent. The fractionation gradient was produced by varying the interaction parameters, γ_A, for both solvent mixtures during the fractionation procedure. This means that these parameters were calculated for every LLE by the solution of the nonlinear system of equations describing the LLE. This is possible because the mass of every fraction was known from the

experiments. For the remaining parameters, the following values were assumed for solvent mixture 1:

$$\chi_{AP} = 0.427 \text{ K} \quad p_A = 0.1 \tag{66}$$

and for solvent mixture 2:

$$\chi_{AP} = 0.671 \text{ K} \quad p_A = 0.05. \tag{67}$$

The theoretical frameworks were executed for the calculations of the distributions in the intermediate and in the final fractions. In Fig. 16, the calculated mass-average chemical compositions were compared with the experimental data obtained by the one-direction fractionation [75]. Using the solvent mixture 1, the mass-average chemical composition decreases with increasing number of fraction. Using the solvent mixture 2, this property increases with increasing number of fraction. The reason for this finding is the sign of the parameter, γ_A, which is positive for the solvent mixture 1 and negative for the solvent mixture 2. The agreement between the experimental and calculated data is much better for the fractionation in the solvent mixture 1 than in the solvent mixture 2, especially for the fractions with a high fraction number. During the experiments [75] using the solvent mixture 2, evaporation of the solvent was observed. This effect is not taken into account in the theoretical calculations.

In Fig. 17, the experimental [75] and calculated number-average segment numbers are compared. According to the SPF mechanisms, the copolymers having the highest molecular weight will preferentially be in the first fractions, independent of the chosen solvent mixture. Except for the fractions having a very high molecular weight, the proposed theoretical framework is able to model the experiment

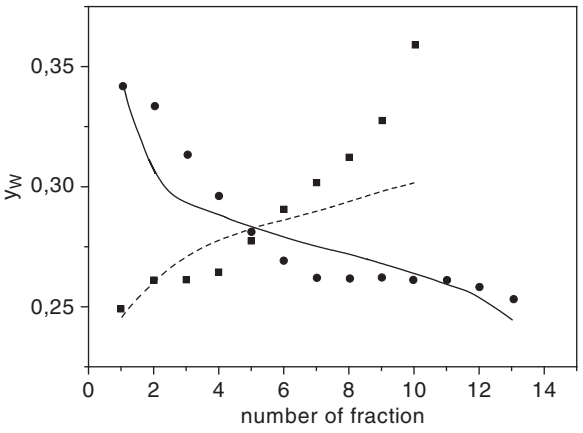

Fig. 16 Comparison of experimental (*symbols*) [75] and calculated (*lines*) mass-average chemical compositions in every fraction after performing a one-direction fractionation using two different solvents: *circles and solid line* solvent mixture 1; *squares and broken line* solvent mixture 2

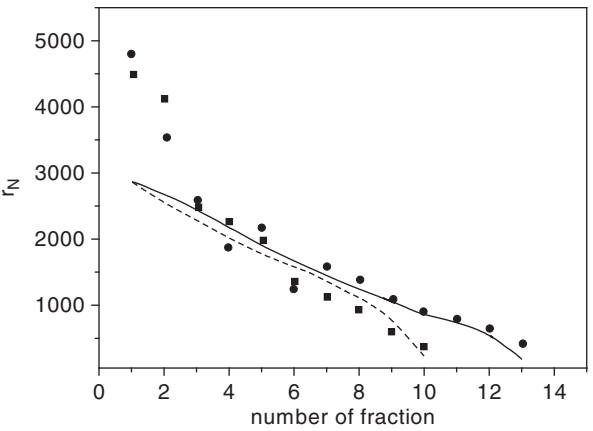

Fig. 17 Comparison of experimental (*symbols*) [75] and calculated (*lines*) number-average segment number in every fraction after performing a one-direction fractionation using two different solvents: *circles and solid line* solvent mixture 1; *squares and broken line* solvent mixture 2

quantitatively. Next, the cross-fractionation should be simulated using the same parameters as for the G^E model. The theoretical results, together with the experimental results [75], are plotted in Fig. 18. Having in mind the approximations introduced in the theoretical framework, it can be notice that the theory is able to model experimental fractionation routines very close to the experimental data.

The effectivity of the fractionation according to the molecular weight can be evaluated by the nonuniformity of the obtained final fractions. This quantity is plotted versus the number of fraction in Fig. 19 for three different fractionation runs, where one is carried out as cross-fractionation and two as one-direction fractionations. Comparing only the one-direction fractionations, it can be recognized that the application of solvent mixture 2 (stars in Fig. 19) leads to a more effective fractionation with respect to the molecular weight, because the fractions have a lower nonuniformity. From the thermodynamic point of view this can be understand by the difference in the Flory–Huggins interaction parameters, χ_{AP} (66, 67). This result demonstrates the important role of the selected solvents. However, the execution of the cross-fraction leads to a strong improvement of the fractionation effectivity, because the nonuniformity is mostly below 0.4. The remarkably high nonuniformity in the last fractions of every intermediate fraction can be explained by the fact that these fractions are the unfractionated remains. In order to improve this situation, more fractionation steps must be carried out.

The enforcement of the copolymer fractionation is motivated by the experimental determination of the two-dimensional distribution function of the original polymer. This is normally done by analysis of the fractionation data (y_{Wi}, r_{Ni}) and construction of the integral distribution function. In Fig. 20, the calculated fractionation data are used for this construction. From Fig. 20a it can be seen that the broadness of the original distribution function with respect to the molecular weight can only be obtained by cross-fractionation. This theoretical result agrees with the

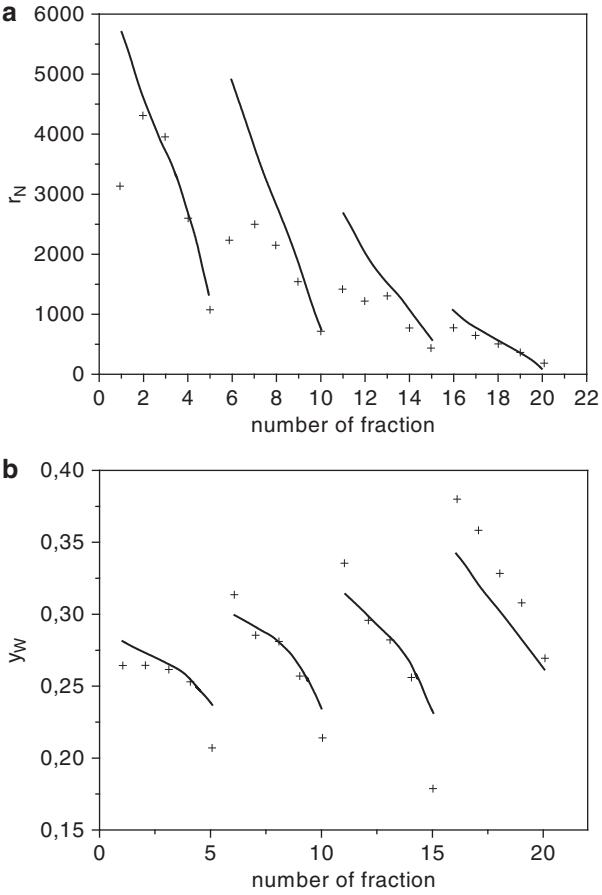

Fig. 18 Comparison of experimental [75] (*symbols*) and calculated (*lines*) cross-fractionations: (**a**) fractionation with respect to the molecular weight, (**b**) fractionation with respect to the chemical composition

experimental observation [75]. Although both one-direction fractionations lead to very close results, they do not find the high molecular weight part of the distribution of the original copolymer. Analyzing the fractionation according to the chemical heterogeneity (Fig. 20b), one can find that the cross-fractionation in comparison to the one-direction fractionation improves the obtained integral distribution function of the original copolymer; however, the complete distribution function could not be recovered. From the thermodynamic point of view, the reason is the selection of the corresponding solvent mixtures. The result could be improved by using a solvent mixture having a larger difference in the parameter γ_A. Again, both one- direction fractionations lead to similar results, but they are not able to reproduce the correct original distribution according to the chemical heterogeneity. If the copolymer

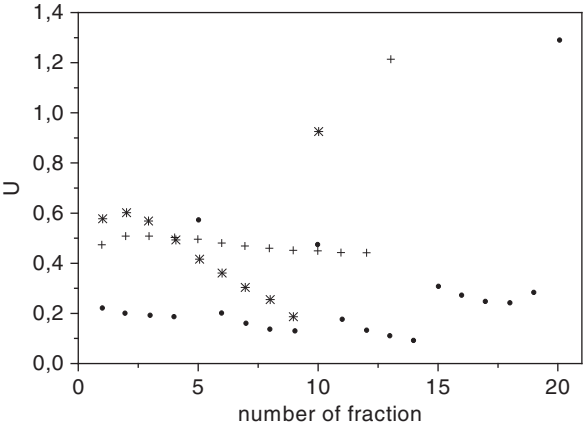

Fig. 19 Comparison of three different fractionation methods: *circles* cross-fractionation, *crosses* successive precipitation fractionation using solvent mixture 1, and *stars* successive precipitation fractionation using solvent mixture 2

fractionation is utilized for analytical purposes, cross-fractionation should be performed, where not only the production of more fractions, but also the application of two different solvent mixtures lead to a significant improvement in the determination of the distribution related to both polydispersities.

In summary, the developed method based on continuous thermodynamics to simulate successive fractionations with respect to the molecular weight and chemical composition is verified by comparison with experimental data, and can be applied for the optimization of a given fractionation problem for analytical and preparative purposes.

3.3 Baker–Williams Fractionation

The most important feature of the BW fractionation method is the high effectivity, especially for analytical purposes. Application of the computer simulation permits the investigation of various effects in the field of column fractionation regarding the effectivity. The simulations were carried out using a copolymer with the following specifications:

$$r_N = 100 \quad k = 1 \quad \varepsilon = 0.3 \quad y_W = 0.5 \quad \alpha = \beta = 4. \tag{68}$$

The selected parameters in the G^E model (5) describing the solvent mixtures are:

$$\begin{aligned} &r_A = 1 \quad \chi_{AP} = 150\ \text{K} \quad p_A = 0 \quad \gamma_A = 0.5 \\ &r_B = 1 \quad \chi_{BP} = 250\ \text{K} \quad p_B = 0 \quad \gamma_B = 1 \\ &\chi_{AB} = 500\ \text{K}. \end{aligned} \tag{69}$$

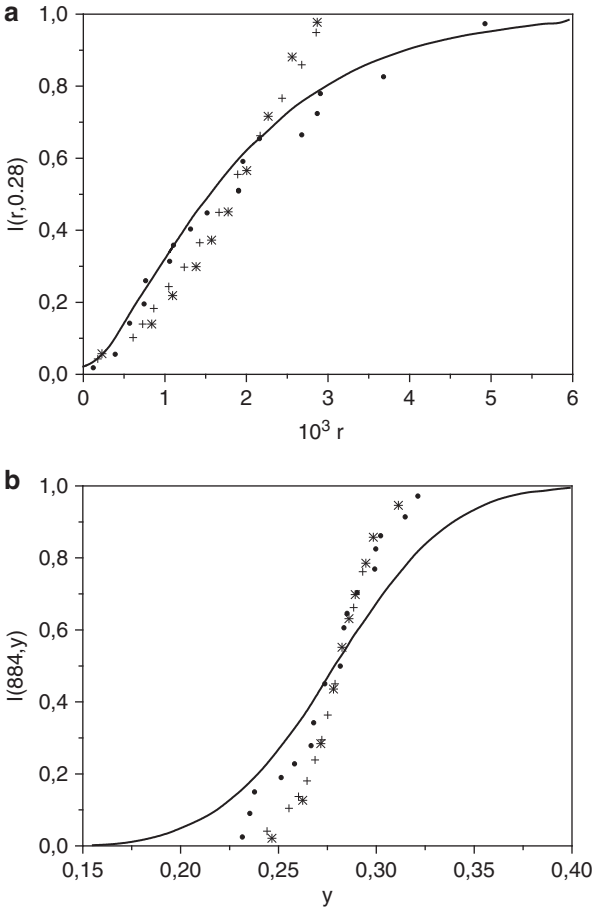

Fig. 20 Comparison of three different fractionation methods: *circles* cross-fractionation, *crosses* successive precipitation fractionation using solvent mixture 1, and *stars* successive precipitation fractionation using solvent mixture 2, with regard to the integral distribution of the original copolymer by (**a**) molecular weight, and (**b**) chemical composition. The *lines* represent the distribution of the original copolymer

For the simulation of the BW column, the operative parameters must also be fixed:

$$X_{0,0}^{\mathrm{F}} = 0.02 \quad m_{\mathrm{P}} = 2 \quad m_{\mathrm{Max}} = 8 \quad Z_{0,0}^{*} = 0.1 \quad v^{*} = 30. \tag{70}$$

Because the copolymers have a different broadness of the distribution according to the Stockmayer theory (15) or according to (16), different temperature and concentration gradients were established in the column. If the original copolymer

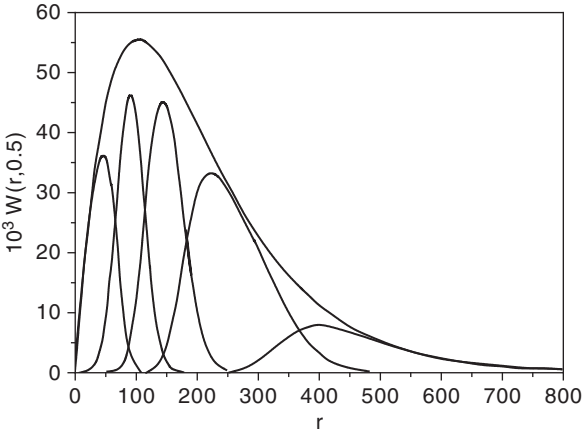

Fig. 21 Simulation results for the Baker–Williams column according to the molecular weight, where the original polymer has a two-dimensional distribution according (16)

is described using the Stockmayer distribution function (15), the operative conditions are:

$$T_0 = 480\ \text{K} \quad \Delta T = 2.5 \quad v_{\text{Max}} = 33 \quad Z^* = 0.25. \tag{71}$$

If the original copolymer is described by the distribution function given in (16), the operative conditions are:

$$T_0 = 400\ \text{K} \quad \Delta T = 5 \quad v_{\text{Max}} = 75 \quad Z^* = 0.4. \tag{72}$$

Figure 21 represents the simulation results for the BW run, where five fractions are formed having an equal amount of the original polymer with a distribution according (16). The obtained fractions show a clearly lower polydispersity than the fractions obtained by successive fractionation methods. The maxima of the distribution functions for the fractions are very close to the original distribution function. This permits an accurate determination of the original distribution function. The last fraction in Fig. 21 has a relative large nonuniformity. However, this can be improved very easily by making more fractions from this material. One advantage of the BW column is the possibility to vary the amount of polymer in the corresponding fraction arbitrarily, without any limits given by the thermodynamics or by the operative parameters of the column. Rätzsch et al. [50] simulated the fractionation of homopolymers having Schulz–Flory distribution functions. They could obtain fractions having a nonuniformity smaller then 0.01. This value could not be reached if copolymers were considered. Usually, the nonuniformities lie between 0.01 and 0.05 for copolymers.

In Fig. 22, the fractionation effect of the BW method with respect to the chemical composition is plotted for a copolymer having a distribution function

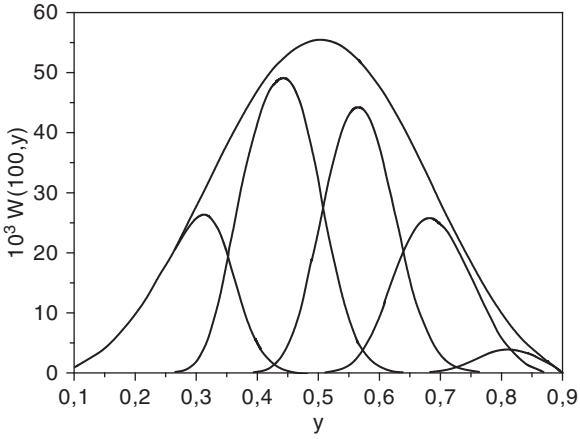

Fig. 22 Simulation results for the Baker–Williams column according to the chemical composition, where the original polymer has a two-dimensional distribution according to (16)

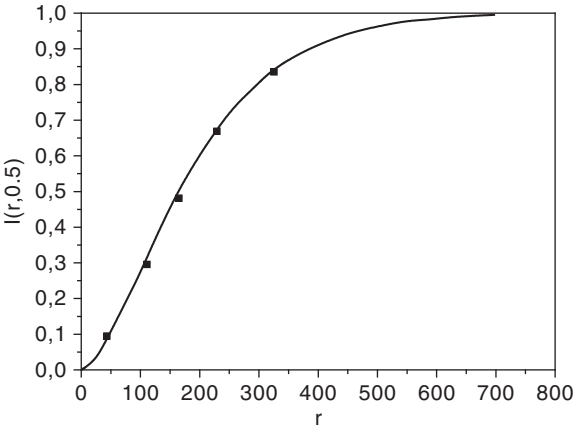

Fig. 23 Simulation results of the Baker–Williams column for a copolymer having a distribution according to (15), where the *symbols* show the fractionation data and the *line* represents the original distribution

given in (16). Again, the application of a BW column leads to a strong improvement in the fractionation effectivity in comparison with the stepwise methods.

The high fractionation effectivity allows correct estimation of the initial copolymer distribution (15) according the molecule weight if only five fractions are formed (Fig. 23). Copolymers distributed according to the Stockmayer distribution function (15) are characterized by a relatively small polydispersity with respect to the chemical composition. In contrast, copolymers showing a distribution given in

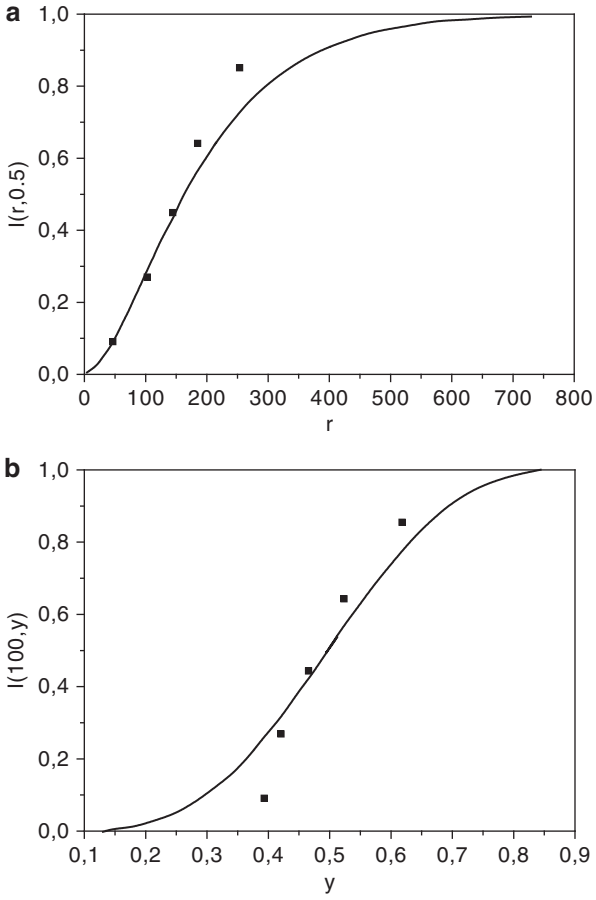

Fig. 24 Simulation results of the Baker–Williams column for a copolymer having a distribution according to (16) with respect to the molecular weight (**a**) and the chemical composition (**b**), where the *symbols* show the fractionation data and the *lines* represent the original distribution

(16) have a broader distribution with respect to the chemical heterogeneity, but the same broadness related to the molecular weight. In Fig. 24, the integral distribution functions constructed from the fractionation data for a copolymer with this distribution function is plotted. From the integral distribution function $I(r, 0.5)$, it can be seen that five fractions are not sufficient to yield the correct original function. Deviation can be found at higher molecular weights (Fig. 24a). The distribution $I(100, y)$ obtained from the fractionation data is also too narrow in comparison with the original distribution (Fig. 24b), where deviations occur at high and at low values of the chemical composition. This result reflects the complex superposition of both kinds of polydispersity.

Rätzsch et al. [50] found by the simulation of the fractionation of homopolymers in the BW column a practical linear relationship between the number of maximal

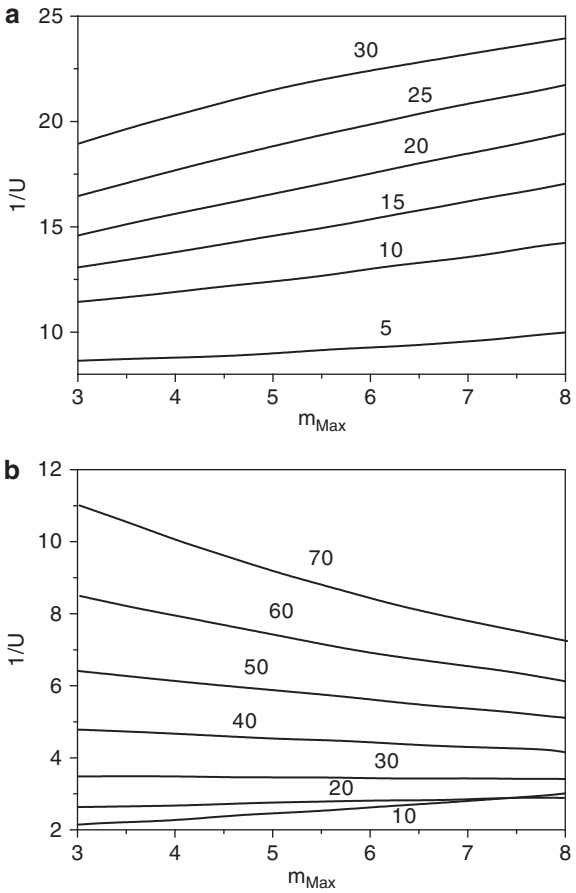

Fig. 25 Simulation results for the Baker–Williams column for different values of the maximal plate number in the column using (15) (**a**) and (16) (**b**) for the feed distribution of the copolymer. The *numbers* are the considered volume element

theoretical plates in the column, m_{Max}, and the reciprocal of the nonuniformity of the obtained fractions. The slope of this relationship was always positive and increased with increasing number of the considered volume element. Figure 25 shows a plot of the reciprocal of the nonuniformity of the copolymer in the corresponding volume element versus the number of theoretical plates established in the column. The results (Fig. 25a) obtained with the copolymer of Stockmayer feed distribution (15) are very similar to those found for the fractionation of homopolymers [50]; however, the slope of the curves are smaller for copolymers than for homopolymers. The number of theoretical plates has a larger impact on the fractionation of homopolymers than on the fractionation of copolymers. Caused by a broader distribution of (16) in comparison with (15), the sign of slope of the

studied relation depends, in this case, on the volume element studied (Fig. 25b). A positive slope can only be found at the beginning of the fractionation, meaning lower numbers of the volume element. With increasing liquid stream (increasing number of volume element), the sign of the slope changed to negative, even though the liquid stream was divided into more volume elements.

In order to study this unexpected phenomena further, the distribution functions in the sol phase of a selected volume element ($v = 30$) traveling through the BW column was investigated. For this reason, simulations of a copolymer having a feed distribution given in (16) for columns differing in the number of theoretical plates (m_{Max}) were performed. The simulation results are depicting in Fig. 26. Increasing the length of the column leads to a more effective fractionation of both

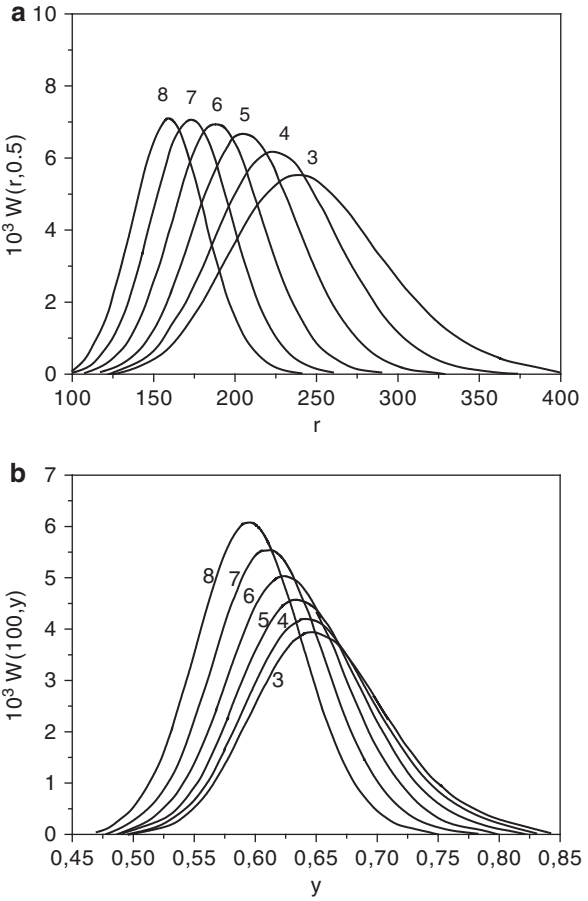

Fig. 26 Distribution of the sol phase with respect to the segment number (**a**) and the chemical composition (**b**) in volume element 30 traveling through the Baker–Williams column with different numbers of maximal theoretical plates m_{Max} (*numbers* in the figure). The original distribution matches (16)

heterogeneities. With increasing length of the column (increasing number m_{Max}) the maxima of the distribution function $W(r, 0.5)$ and the distribution function $W(100,y)$ shift for the observed volume elements to lower values and both distribution functions become narrower. For the volume element $v = 70$ moving through the column, the length of the column has the opposite effect. The practical consequence is the relative large polydispersity in the large fraction.

Increasing the number of theoretical plates, m_{Max}, allows establishing a more flat temperature gradient in the column for the same fractionation results.

In summary, the suggested theoretical model can be applied to answer different questions arising about the efficiency of copolymer fractionation performed in BW columns. This type of column is mostly used for analytical purposes.

3.4 Continuous Polymer Fractionation

CPF has been especially developed to produce large fractions in a relatively short time frame and can be applied for preparative purposes. All traditional procedures, especially the stepwise methods, require a low polymer concentration for good efficiency, and large amounts of solutions must be handled to obtain sufficient material. With this fractionation method, the initial copolymer is divided into two fractions, where these fractions can be used again as feed for the next fractionation run. For homopolymers, this fractionation method is a useful tool for cutting the short molecular weight parts or the extremely high molecular weight parts from the desired product. In the case of copolymers, those with extremely high or low values for the chemical composition can also be removed from the product. The simulation method suggested above is now applied for the optimization of the CPF. This optimization is always done by variation of the parameters describing the column and keeping all others constant. The copolymer (68) used for the simulations and the parameters of the G^{E} model (69) are identical to those used for the simulation of the BW columns. The standard parameter set for the operating conditions is:

$$\begin{aligned} X^{\mathrm{FD}} = 0.11 \quad Z^{\mathrm{FD}} = 0.5 \quad Z^{\mathrm{EA}} = 0.15 \quad n^{\mathrm{FD}}/n^{\mathrm{EA}} = 0.1 \\ m_{\mathrm{Max}} = 6 \quad m_{\mathrm{FD}} = 3 \quad T = 520\ \mathrm{K} \quad T_{\mathrm{condenser}} = 500\ \mathrm{K}. \end{aligned} \tag{73}$$

For example, the calculated fractionation data for four CPF runs are collected in Table 1, where the initial polymer distribution was a Stockmayer distribution (15). For the fractionation, four CPF runs were simulated in which the obtained gel fractions were directly used as new feed phase.

The data in Table 1 make it clear that no significant fractionation according to the chemical heterogeneity took place. However, the fractionation effect with respect to the molecular weight is characterized by a high effectivity. Except for the first fraction, all other fractions have a nonuniformity lower than 0.06, similar to the results obtained for the simulation of the BW column. The nonuniformities are

Table 1 Calculated fractionation data for CPF, where the original copolymer has a Stockmayer distribution (15)

Fraction no.	T (K)	y_W	r_N	U
1	520	0.49567	74.8	0.673
2	530	0.50651	216.8	0.058
3	540	0.50696	266.0	0.039
4	550	0.50766	311.7	0.037
5	550	0.51159	427.9	0.071

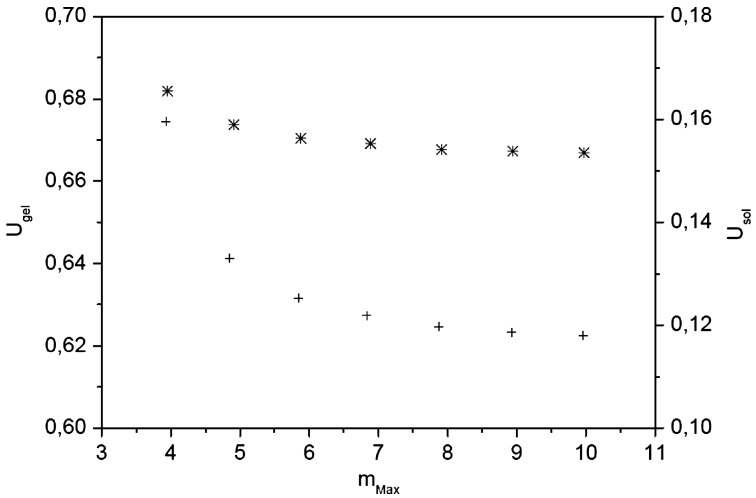

Fig. 27 Influence of the number of theoretical plates, m_{Max}, on the fractionation efficiency with respect to the segment number of CPF, if the original copolymer distribution is given by (15). The *stars* represent the values of the sol fraction and the *crosses* the values from the gel fractions

slightly higher for copolymers in comparison with homopolymers [49], showing the influence of chemical heterogeneity on the fractionation with respect to the molecular weight, even if the polydispersity with respect to the chemical composition is small. The following optimization procedure aims for a much stronger fractionation effect with respect to the chemical composition and, at the same time, to keep the effectivity for the fractionation with respect to the molecular weight. Furthermore, during the optimization it is assumed that the both solvents and the thermodynamic properties, expressed by the parameter of the G^E model, cannot be changed. This means we focus our attention on the optimization of the operative conditions, which can also be changed in practice.

First, the influence of the number of theoretical plates of the CPF column is studied (Fig. 27). The discussion can be done using the nonuniformities in the resulting sol and gel phases. Independently of the isolated phase (sol or gel), the nonuniformity decreases with increasing number of theoretical plates present in the CPF column. However, the decline is only very limited if the column has more

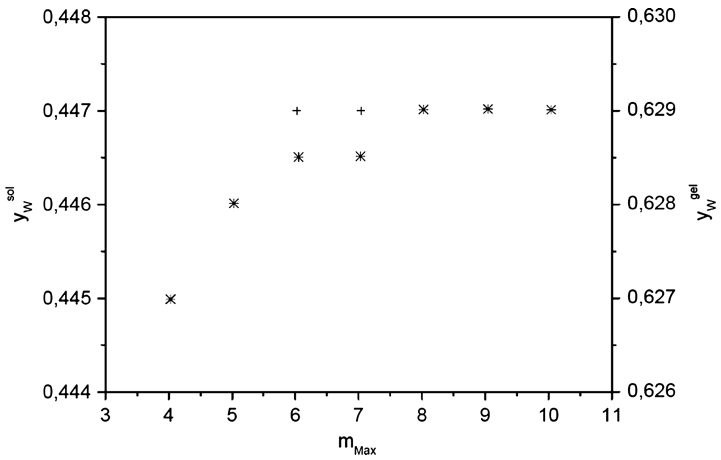

Fig. 28 Influence of the number of theoretical plates, m_{Max}, on the fractionation efficiency with respect to chemical composition of CPF, if the original copolymer distribution is given by (16). The *stars* represent the values of the sol fraction and the *crosses* the values from the gel fractions

than six theoretical plates. This result was also obtained by Rätzsch et al. [49] for the fractionation of homopolymers.

In order to study the influence of the number of theoretical plates on the fractionation according to the chemical composition, simulations using (16) as feed distribution function were performed, because this type of distribution function models a broader distribution. The obtained results are given in Fig. 28. Again, theoretical plates having numbers greater than six do not contribute strongly to the fractionation effect in the CPF column. For practical fractionation, it can recommend to use a column having six theoretical plates.

The next question arising in relation to the CPF column is where the feed phase should be put in the column. The quantity is represented in the theoretical framework by the parameter m_{FD}.

Simulations of the CPF column were carried out for the copolymer with a feed distribution of (16) at different places for the feed input. The results are depicted in Fig. 29 for the fractionation with respect to the segment number and in Fig. 30 for the fractionation with respect to the chemical composition. With increasing m_{FD}, the nonuniformity in the sol as well as in the gel decreases (Fig. 29). Analyzing the fractionation according to the chemical composition leads to the same result (Fig. 30). However, feed input at plate number 4 ($m_{\mathrm{FD}} = 4$) cannot be recommended because the polymer concentration on the plate above will be too small. The most effective fractionation can be expected if the feed is added a little above the middle of the columns. If the column with $m_{\mathrm{Max}} = 6$ is used, then the feed should be added at $m_{\mathrm{FD}} = 3$.

The next operative parameter is the ratio between the amount of feed copolymer solution and the amount of extraction solvent, meaning the working point (Fig. 6).

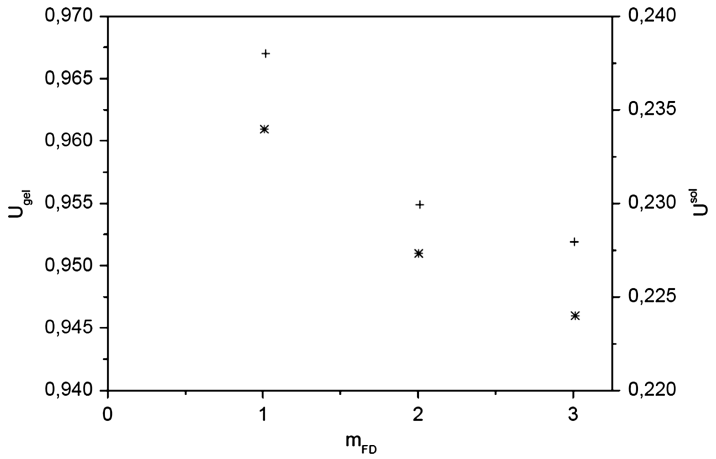

Fig. 29 Estimation of the optimal feed plate for the CPF column for the fractionation according the molecular mass if the original polymer is described by (16). The *stars* represent the values of the sol fraction and the *crosses* the values from the gel fractions

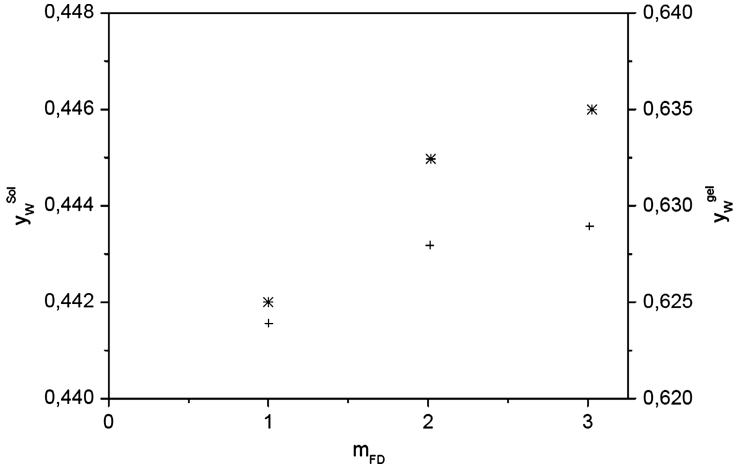

Fig. 30 Estimation of the optimal feed plate for the CPF column for the fractionation according the chemical composition if the original polymer is described by (16). The *stars* represent the values of the sol fraction and the *crosses* the values from the gel fractions

The calculation results obtained by simulation of the fractionation of a copolymer having the initial distribution function given in (16) for different values of n^{FD}/n^{EA} are shown in Fig. 31. The nonuniformity decreases in the gel as well in the sol phase if more extraction agent is used (Fig. 31a). The fractionation according to the chemical composition shows an identical trend. The finding can be explained by

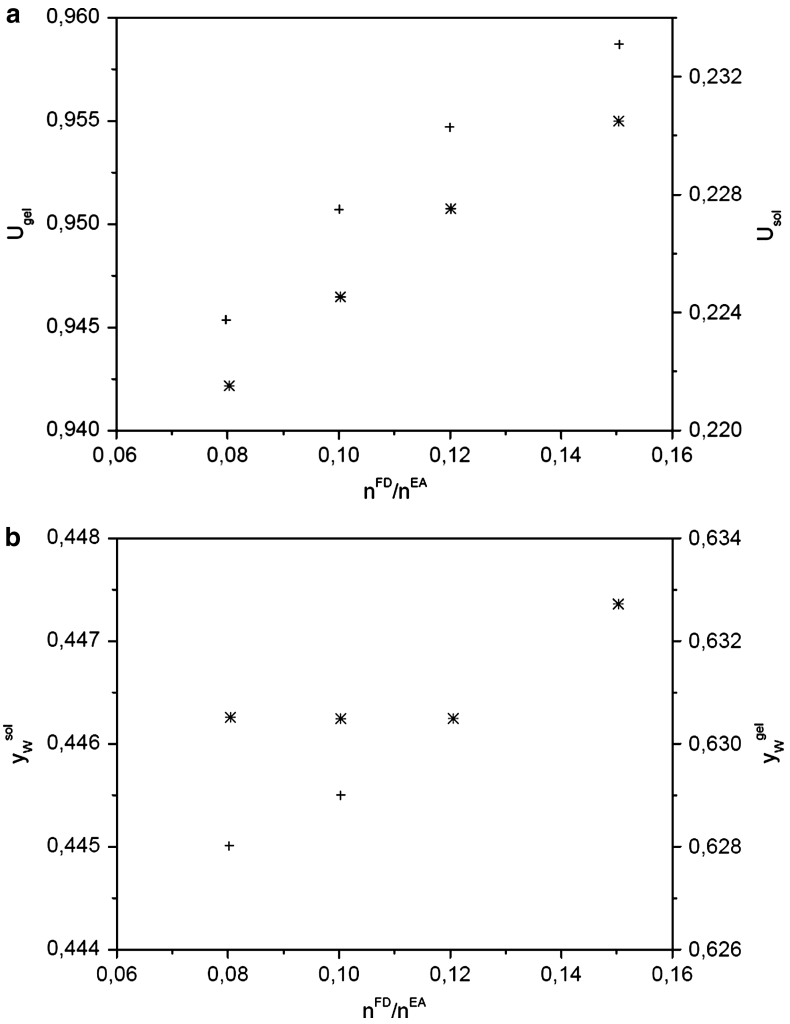

Fig. 31 Influence of working point on the CPF fractionation effect with respect to the molecular weight (**a**) and the chemical composition (**b**) for a copolymer having an initial distribution given by (16). The *stars* represent the values of the sol fraction and the *crosses* the values from the gel fractions

the dilution effect. However, increasing the amount of extraction agent leads to a decrease in the polymer amount present in the column and hence in the produced fraction. In this situation, a compromise between high fractionation effect and the amount of copolymer in the fractions has to be found.

The next operative parameter, which can be optimized by simulation, is the cooling temperature at the condenser. This parameter is also optimized by simulations of the CPF column, where a copolymer is fractionated with a feed distribution

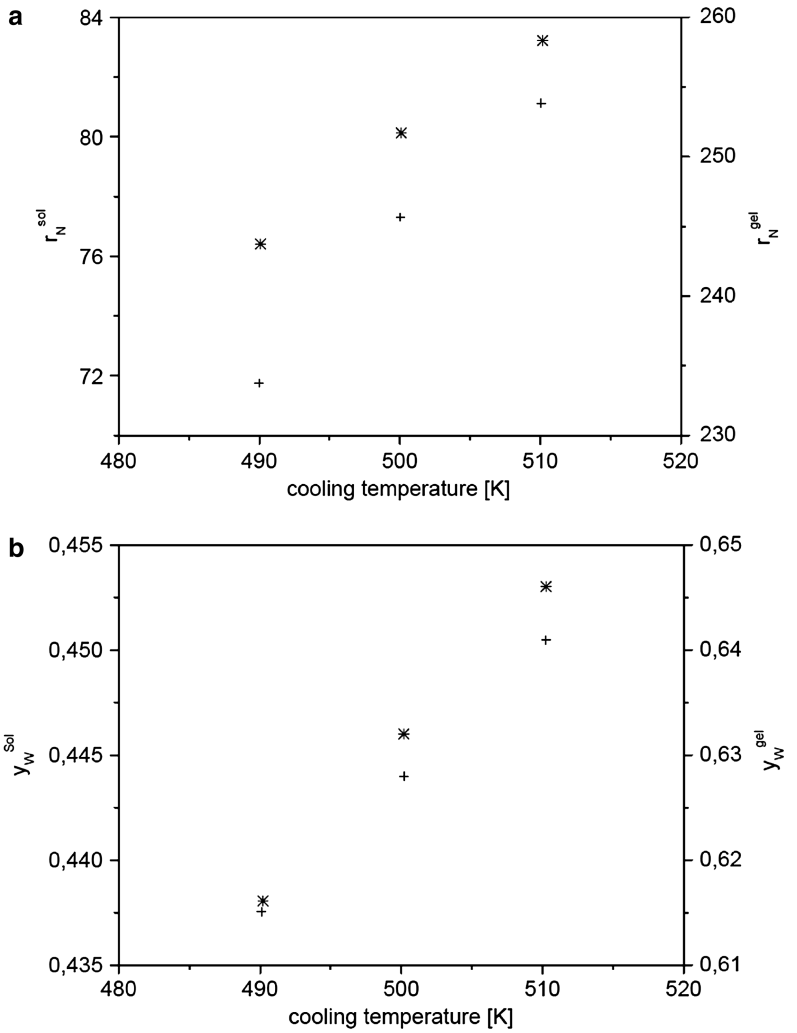

Fig. 32 Influence of cooling temperature in the condenser on the CPF fractionation effect with respect to the molecular weight (**a**) and the chemical composition (**b**) for a copolymer having an initial distribution given by (16). The *stars* represent the values of the sol fraction and the *crosses* the values from the gel fractions

given in (16). The simulation results are demonstrated in Fig. 32 for the fractionation of both polydispersities. From this figure, it can be seen that the optimal temperature in the condenser depends on the phase that forms the final fraction. If the fraction is to be isolated from the sol phase, then the condenser should work at temperatures as low as possible. However, if the fraction is to be taken from the gel phase, the condenser should not be used. These results are of practical importance

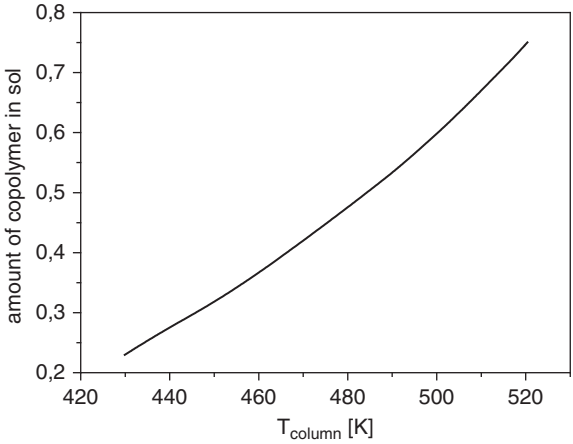

Fig. 33 The relationship of the amount of copolymer present in the sol phase and the temperature in the column

in the case where the CPF is applied for cutting the short or the large molecular weight parts from a synthetic polymer in order to tailor the material properties.

From the calculation results of the stepwise fractionation methods, it is known that the amount of polymer should by equal in all fractions. In CPF, the amount of polymer segments depends on the chosen working point (n^{FD}/n^{EA}) and the temperature in the column. In Fig. 33, the relationship between the temperature in the column and the amount of polymer present in the sol phase is shown.

Using all this knowledge from the simulations above, the following so-called optimized parameters for the CPF column:

$$\begin{aligned} &X^{FD} = 0.11 \quad Z^{FD} = 0.5 \quad Z^{EA} = 0.15 \quad n^{FD}/n^{EA} = 0.08 \\ &m_{Max} = 6 \quad m_{FD} = 3 \quad T_{condenser} = 430\ \text{K} \end{aligned} \tag{74}$$

were used to fractionate a copolymer into five fractions by four fractionation runs. The temperature for each fractionation run was selected in such a way that in every fraction there was nearly the same amount of polymer.

The results for this fractionation are presented in Table 2, Fig. 34, and Fig. 35. The differences between the original operating parameters (73) to the optimized parameters (74) are, first, that the n^{FD}/n^{EA} ratio is changed slightly and, second, that the temperature gradient is much more pronounced. The temperature at the condenser is changed from 520 to 430 K, whereby the temperature in the column is raised, especially for the last fractionation run. Similar to the results found for stepwise fractionation, the most important feature for an effective fractionation in column is also that the polymer is equally distributed in the corresponding fractions.

The improvement can be recognized clearly if the fractionation with respect to the chemical composition is analyzed (Table 2 and Fig. 35). The fractionation

Table 2 Calculated fractionation data for CPF, where the original copolymer has a feed distribution given by (16). The operating conditions are given in (74)

Fraction no.	T (K)	y_W	r_N	U
1	430	0.387	43.8	0.992
2	480	0.435	112.8	0.381
3	530	0.502	157.2	0.295
4	580	0.589	222.2	0.214
5	580	0.698	323.1	0.149

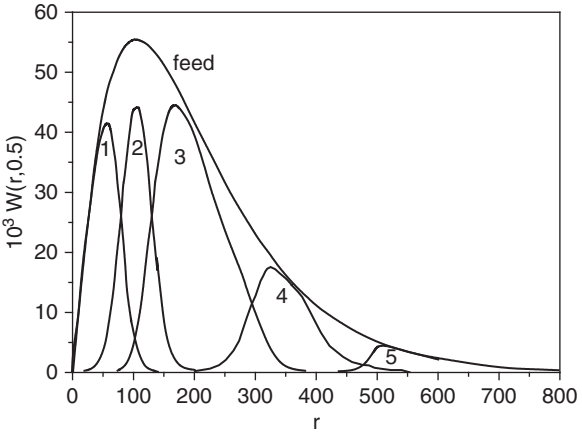

Fig. 34 CPF calculations using optimized operative parameters, where the *numbers* indicate the fraction number

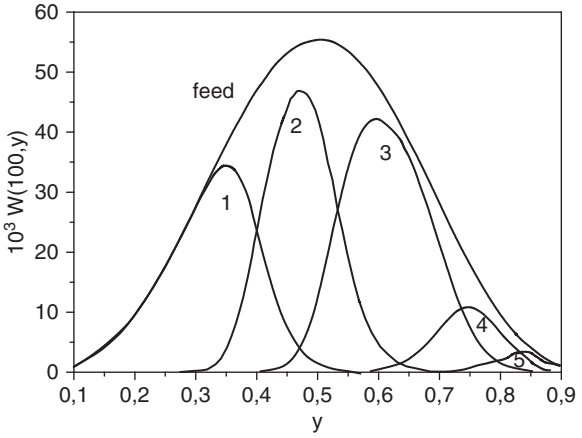

Fig. 35 CPF calculations using optimized operative parameters, where the *numbers* indicate the fraction number

according both polydispersities can be characterized by a high effectivity, which can been seen in Figs. 34 and 35.

In summary, both fractionation methods using columns can be applied for the fractionation of copolymers; however, the separation efficiency for the fractionation with respect to the molecular weight is lower than for the fractionation of homopolymers. For the development of further fractionation methods for copolymers, it is suggested that the CPF column is also used for fractionation in two directions, similar to the cross-fractionation. This can be realized experimentally very simply by changing the solvent mixture in the different runs, necessary to produce different fractions.

4 Summary

For the first time, a theoretical framework for the fractionation of statistical copolymers using successive fractionation methods and columns is introduced, taking into account the polydispersity with respect to molecular weight and chemical composition.

The application of this theoretical framework based on continuous thermodynamics allows the investigation of operating parameters (solvent gradient, temperature gradient, features of the fractionation column, fractionation strategy) on the efficiency of the fractionation, where the two-dimensional distribution of statistical copolymers is completely taken into account. From the thermodynamic point of view, copolymer fractionation is the successive establishing of LLE for suitable solutions of the polymer to be fractionated. Similar to the theoretical description of distillation or extraction columns in chemical engineering, the column is divided into theoretical stages. Assuming an LLE on each theoretical stage, the polymer fractionation can be modeled using phase equilibrium thermodynamics.

From the results of calculations carried out for the successive cross-fractionations, where in principal four different fractionation strategies are possible, it can be concluded that the fractionations in both solvent mixtures should be performed using SSF, meaning that the obtained sol phase should always be taken as a fraction.

During simulation of the fractionation in columns, such as the BW column or the CPF column, the influence of the operative conditions on the fractionation effectivity was investigated. For the simulation of the BW column, the main focus was the analytical purpose and in the simulation of the CPF column, the focus was the preparative purpose. Similar to the results found for the stepwise fractionation, the most important feature for an effective fractionation in column is also that the polymer is equally distributed in the corresponding fractions. This can be achieved by a suitable chosen concentration or temperature gradient, or both.

Acknowledgment Sincere thank is given to Dr. Heike Kahl for support in preparation of the manuscript.

References

1. Rätzsch MT, Kehlen H (1989) Continuous thermodynamics of polymer systems. Prog Polym Sci 14:1–46
2. Wohlfarth C, Rätzsch MT (1990) Continuous thermodynamics of copolymer systems. Adv Polym Sci 98:49–114
3. Rätzsch MT, Kehlen H, Browarzik D (1985) Liquid–liquid equilibrium of polydisperse copolymer solutions. Multivariate distribution functions in continuous thermodynamics. J Macromol Sci Chem A 22:1679–1680
4. Rätzsch MT, Browarzik D, Kehlen H (1989) Refined continuous thermodynamic treatment for the liquid–liquid equilibrium of copolymer solutions. J Macromol Sci Chem A 26:903–920
5. Rätzsch MT, Kehlen H, Browarzik D, Schirutschke M (1986) Cloud-point curves for the system copoly(ethylene-vinyl acetate) plus methylacetate. Measurement and prediction by continuous thermodynamics. J Macromol Sci Chem A 23:1349–1361
6. Rätzsch MT, Browarzik D, Kehlen H (1990) Liquid–liquid equilibrium of copolymer solutions with broad and asymmetric chemical distribution. J Macromol Sci Chem A 27:809–830
7. Browarzik C, Browarzik D, Kehlen H (2001) Phase-equilibrium calculation for solutions of poly(ethylene-co-vinyl acetate) copolymers in supercritical ethylene using a cubic equation of state. J Supercrit Fluids 20:73–88
8. Browarzik D, Rätzsch MT, Wohlfarth C (2003) High pressure phase equilibria in the system ethylene + vinylacetate + (ethylene vinylacetate) copolymer treated by continuous thermodynamics. Acta Polymerica 40:457–462
9. Koningsveld R (1970) Preparative and analytical aspects of polymer fractionation. Adv Polym Sci 7:1–69
10. Tung LH (ed) (1977) Fractionation of synthetic polymers. Marcel Dekker, New York
11. Koningveld R, Stockmayer WH, Nies E (2001) Polymer phase diagrams. Oxford University Press, Oxford
12. Provder T, Whited M, Huddleston D, Kuo CY (1997) Characterization of compositional heterogeneity in copolymers and coatings systems by GPC/FTIR. Prog Org Coating 32:155–165
13. Pratt JA, McHugh MA (1996) Supercritical-fluid fractionation of poly(ethylene-co-acrylic acid). J Supercrit Fluids 9:61–66
14. Scholsky KM, O'Connor KM, Weiss CS, Krukonis VJ (1987) Characterization of copolymers fractionated using supercritical fluids. J Appl Polym Sci 33:2925–2934
15. Pratt JA, Lee SH, McHugh MA (1993) Supercritical fluid fractionation of copolymers based on chemical composition and molecular weight. J Appl Polym Sci 49:953–966
16. Glöckner G, Kroschwitz H, Meissner C (1982) HP precipitation chromatography of styrene–acrylonitrile copolymers. Acta Polymerica 33:614–616
17. Glöckner G, van den Berg JHM, Meijerink NLJ, Scholte TG, Koningsveld R (1984) Size exclusion and high-performance precipitation liquid chromatography of styrene–acrylonitrile copolymers. Macromolecules 17:962–967
18. Glöckner G, van den Berg JHM (1987) Copolymer fractionation by gradient high-performance liquid chromatography. J Chromatogr 384:135–144
19. Glöckner G, Ilchmann D (1984) Hochdruck-Fällungschromatographie von α-Methylstyren/Acrylnitril-Copolymeren. Acta Polymerica 35:680–683
20. Mori S, Uno Y (1987) Operational variables for the separation of styrene–methyl methacrylate copolymers according to chemical composition by liquid adsorption chromatography. Anal Chem 59:90–94
21. Teramachi S, Hasegawa A, Shima Y, Akatsuja M, Nakajima M (1979) Separation of styrene–methyl acrylate copolymer according to chemical composition, using high-speed liquid chromatography. Macromolecules 12:992–996

22. Glöckner G (1987) Quantitative aspects of gradient HPLC of copolymers from styrene and ethyl methacrylate. Chromatographia 23:517–524
23. Glöckner G, Stickler M, Wunderlich W (1987) Investigation of copolymers of styrene and ethyl methacrylate by size exclusion chromatography and gradient HPLC. Fresenius Z Anal Chem 328:67–81
24. Glöckner G, Barth HG (1990) Use of high-performance liquid chromatography for the characterization of synthetic copolymers. J Chromatogr 499:645–654
25. Glöckner G, Stickler M, Wunderlich W (1989) Separation of *stat*-copoly(styrene/2-methoxyethyl methacrylate) samples according to composition by gradient high-performance liquid chromatography. J Appl Polym Sci 37:3147–3161
26. Xu Z, Yuang P, Zhong J, Jiang E, Wu M, Fetters LJ (1989) The characterization of a poly (ethylene terephthalate)–poly(tetramethylene ether) multiblock copolymer via cross fractionation and size exclusion chromatography. J Appl Polym Sci 37:3195–3204
27. Stejskal J, Strakova D, Kratochvil P, Smith SD, McGrath JE (1989) Chemical composition distribution of a graft copolymer prepared from macromonomer: fractionation in demixing solvents. Macromolecules 22:861–865
28. Dong Q, Fan ZQ, Fu ZS, Xu JT (2007) Fractionation and characterization of an ethylene–propylene copolymer produced with a $MgCl_2/SiO_2/TiCl_4$ diester type Ziegler–Natta catalyst. J Appl Polym Sci 107:1301–1309
29. Podešva J, Stejskal J, Prochăzka O, Špaček P, Enders S (1993) Fractionation of a statistical copolymer in a demixing-solvent system: theory and experiment. J Appl Polym Sci 48:1127–1135
30. Kakugo M, Miyatake T, Mizunuma K (1991) Chemical composition distribution of ethylene-1-hexane copolymer prepared with $TiCl_3$–$Al(C_2H_5)_2Cl$ catalyst. Macromolecules 24:1469–1472
31. van Asten AC, van Dam RJ, Kok WT, Tijssen R, Poppe H (1995) Determination of the compositional heterogeneity by polydisperse polymer samples by the coupling of size-exclusion chromatography and thermal field-flow fractionation. J Chromatogr A 703:245–263
32. Hwang SW, Kim E, Shin C, Kim JH, Ryu DY, Park S, Chang T (2007) Unusual sensitivity of closed-loop phase behavior to chain size and distribution. Macromolecules 40:8066–8070
33. Ogawa T (1990) Fractionation and characterization of polyacetal copolymers by column elution method. J Appl Polym Sci 40:1519–1527
34. Zhang M, Lynch DT, Wanke SE (2000) Characterization of commercial linear low-density polyethylene by TREF-DSC and TREF-SEC cross fractionation. J Appl Polym Sci 75:960–967
35. Kong J, Fab X, Xie Y, Qiao W (2004) Study on molecular chain heterogeneity of linear low-density polyethylene by cross-fractionation of temperature rising elution fractionation and successive self-nucleation/annealing thermal fractionation. J Appl Polym Sci 94:1710–1718
36. van den Glöckner G, Berg JHM, Meijerink NLJ, Scholte TG, Koningsveld R (1984) Two-dimensional analysis of copolymers by size-exclusion chromatography and gradient-elution reversed-phase precipitation chromatography. J Chromatogr 317:615–624
37. Cho KH, Park YH, Jeon SJ, Kim WS, Lee DW (1997) Retention behavior of copolymers in thermal field-flow fractionation and gel permeation chromatography. J Liq Chromatogr Relat Technol 20:2741–2756
38. Nakano S, Goto Y (1981) Development of automatic cross fractionation: combination of crystallizability fractionation and molecular weight fractionation. J Appl Polym Sci 26:4217–4231
39. Springer H, Hengse A, Hinrichsen G (1990) Fractionation and characterization of a 1-butene linear low density polyethylene. J Appl Polym Sci 40:2173–2188
40. Baker CA, Williams RJP (1956) A new chromatographic procedure and its application to high polymers. J Chem Soc:2352–2362
41. Barker PE, Hatt BW, Williams AN (1978) Fractionation of a polymer using a preparative-scale continuous chromatograph. Chromatographia 11:487–493

42. Gerrissen H, Roos J, Wolf BA (1985) Continuous fractionation and solution properties of PVC. 1. Continuous fractionation, characterization. Makromol Chemie 186:735–751
43. Kalal J, Marousek V, Svec F (1974) Fraktionierung von Vinylchlorid/Vinylacetat Copolymeren. Angew Makromol Chem 38:45–55
44. Mencer HJ, Kunst B (1978) A modified column method of polymer fractionation. Colloid Polym Sci 256:758–760
45. Wu AH, Prausnitz JM (1990) Fractionation of polydisperse polymer using an antisolvent. Application of continuous thermodynamics. J Appl Polym Sci 39:629–637
46. Rätzsch MT, Kehlen H, Tschersich L (1989) Application of continuous thermodynamics to polymer fractionation. J Macromol Sci Chem A26:921–935
47. Rätzsch MT, Enders S, Tschersich L, Kehlen H (1991) Polymer fractionation calculations using refined free energy relations. J Macromol Sci Chem A28:31–46
48. Rätzsch MT, Kehlen H, Tschersich L, Wolf BA (1991) Application of continuous thermodynamics to polymer fractionation. Pure Appl Chem 63:1511–1518
49. Weinmann K, Wolf BA, Rätzsch MT, Tschersich L (1992) Theory-based improvements of the CPF (continuous polymer fractionation) demonstrated for poly(carbonate). J Appl Polym Sci 45:1265–1279
50. Rätzsch MT, Tschersich L, Kehlen H (1990) Simulation of Baker–Williams fractionation by continuous thermodynamics. J Macromol Sci A27:999–1013
51. Folie B (1996) Single-stage fractionation of poly(ethylene-co-vinyl acetate) in supercritical ethylene with SAFT. AIChE J 42:3466–3476
52. Litmanovich AD, Shtern VY (1967) On the cross-fractionation of copolymers. J Polym Sci C 16:1375–1382
53. Ogawa T, Inaba T (1974) Analysis of the fractionation of ethylene–propylene copolymerization products. J Appl Polym Sci 18:3345–3363
54. Flory PJ (1953) Principles of polymer chemistry. Cornell University Press, Ithaca
55. Barker JA (1952) Cooperative orientation effects in solutions. J Chem Phys 20:1526–1531
56. Stockmayer WH (1945) Distribution of chain lengths and compositions in copolymers. J Chem Phys 13:199–207
57. Becker F, Buback M, Latz H, Sadowski G, Tumakaka F (2004) Cloud-point curves of ethylene-(meth)acrylate copolymers in fluid ethene up to high pressures and temperature – experiment study and PC-SAFT modeling. Fluid Phase Equilib 215:263–282
58. Kleiner M, Tumakaka F, Sadowski G, Latz H, Buback M (2006) Phase equilibria in polydisperse and associating copolymer solutions: poly(ethylene-co-(meth)acrylic acid)–monomer mixture. Fluid Phase Equilib 241:113–123
59. Gross J, Spuhl O, Tumakaka F, Sadowski G (2003) Modeling copolymer systems using the perturbed-chain SAFT equation of state. Ind Eng Chem Res 42:1266–1274
60. Wohlfarth C, Rätzsch MT (1987) Kontinuierliche Thermodynamik des Entmischungsgleichgewichtes: Berechnung der Schattenkurve im System Ethylen + Vinylacetat + (Ethylen-Vinylazetat)-Copolymer. Acta Polymerica 38:156–158
61. Browarzik D, Kehlen H (1996) Stability of polydisperse fluid mixtures. Fluid Phase Equilib 123:17–28
62. Teramachi S, Tomioka H, Sotokawa M (1972) Phase-separation phenomena of copolymer solutions and fractionation of copolymers by chemical composition. J Macromol Sci A6:97–107
63. Teramachi S, Nagasawa M (1968) The fractionation of copolymers by chemical composition. J Macromol Sci A2:1169–1179
64. Rosenthal AJ, White BB (1952) Fractionation of cellulose acetate. Ind Eng Chem 44:2693–2696
65. Teramachi S, Kato Y (1971) Study of the distribution of chemical composition in low-conversion copolymer by cross-fractionation. Macromolecules 4:54–56
66. Teramachi S, Hasegawa A, Hasegawa S, Ishibe T (1981) Determination of chemical composition distribution in a high-conversion copolymer of styrene and methyl acrylate by cross fractionation. Polym J 4:319–323

67. Teramachi S, Hasegawa A, Yoshida S (1982) Comparison of cross fractionation and TLC methods in the determination of the compositional distribution of statistical copolymer. Poly J 14:161–164
68. Spychaj T (1987) Solvent/non-solvent solubility and polarity parameters in fractional separation of oligomers 2. Epoxy resins. Angew Makromol Chem 149:127–138
69. Spychaj T, Hamielec AE (1988) Solvent/non-solvent solubility and polarity parameters in fractional separation of oligomers 2. Styrene–acrylic acid copolymer. Angew Makromol Chem 157:137–151
70. Stejskal J, Kratochvil P (1978) Fractionation of a model random copolymer in various solvent systems. Macromolecules 11:1097–1103
71. Stejskal J, Kratochvil P, Strakova D (1981) Study of the statistical chemical heterogeneity of copolymers by cross fractionation. Macromolecules 14:150–154
72. Bodor G, Dalcolmo HJ, Schröter O (1989) Structural and property correlation of ethylene-α-olefin copolymers. Colloid Polym Sci 267:480–493
73. Arranz F, Sanchez-Chaves M (1985) Chemical heterogeneity of a partially modified dextran with ethyl carbonate groups. Angew Makromol Chem 135:139–149
74. Teramachi S, Fukao T (1974) Cross fractionation of styrene–acrylonitrile copolymer. Polym J 6:532–536
75. Teramachi S, Kato Y (1970) Cross fractionation of styrene–butadiene copolymer. J Macromol Sci A4:1785–1796
76. Smith WV (1970) Precipitation chromatography theory. J Polym Sci A 2(8):207–224
77. Mac Lean DL, White JL (1972) The precipitation chromatographic column: theory, critique and method of design. Polymer 13:124–132
78. Geerissen H, Roos J, Wolf BA (1985) Continuous fractionation and solution properties of PVC, 1. Continuous fractionation, characterization. Makromol Chem 186:735–751
79. Geerissen H, Schützeichel P, Wolf BA (1990) Large scale fractionation of polyethylene by means of the continuous polymer fractionation (CPF) method. Makromol Chem 191:659–670
80. Gosch CI, Haase T, Wolf BA, Kulicke WM (2002) Molar mass distribution and size of hydroxyethyl starch fractions obtained by continuous polymer fractionation. Starch/Stärke 54:375–384
81. Hagenaars AC, Pesce JJ, Bailly C, Wolf BA (2001) Characterization of melt-polymerized polycarbonate: preparative fractionation, branching distribution and simulation. Polymer 42:7653–7661
82. Haberer M, Wolf BA (1995) Continuous fractionation of poly(acrylic acid). Angew Makromol Chem 228:179–184
83. Geerissen H, Roos J, Schützeichel P, Wolf BA (1987) Continuous fractionation and solution properties of PIB. I. Search for the best mixed solvent and first results of the continuous polymer fractionation. J Appl Polym Sci 34:271–285
84. Geerissen H, Schützeichel P, Wolf BA (1987) Continuous fractionation and solution properties of PIB. II. CPF optimization. J Appl Polym Sci 34:287–305
85. Samadi F, Eckelt J, Wolf BA, López-Villanueva FJ, Frey H (2007) Branched versus linear polyisoprene: fractionation and phase behavior. Eur Poly J 43:4236–4243
86. Eckelt J, Haase T, Loske S, Wolf BA (2004) Large scale fractionation of macromolecules. Macromol Mater Eng 289:393–399
87. Xiong X, Eckelt J, Wolf BA, Zhang Z, Zhang L (2006) Continuous spin fractionation and characterization by size-exclusion chromatography for styrene–butadiene block copolymers. J Chromatogr A 1110:53–60
88. Hagenaars AC, Bailly C, Schneider A, Wolf BA (2002) Preparative fractionation and characterization of polycarbonate/eugenol-siloxane copolymers. Polymer 43:2663–2669
89. Schmiedbauer J, Sybert PD (2000) In: Legrand DG, Bendler JT (eds) Handbook of polycarbonate science and technology. Marcel Dekker, New York
90. Schiruschke M (1976) Quellungsmessungen an Hochpolymeren. Diploma thesis, Technical University Merseburg